Assimilation of SMAP disaggregated soil moisture and Landsat land surface temperature to improve FAO-56 estimates of ET in semi-arid regions

Abdelhakim Amazirh[a,*], Salah Er-Raki[a,b], Nitu Ojha[c], El houssaine Bouras [b,c], Vincent Rivalland[c], Olivier Merlin[c]. Abdelghani Chehbouni[a,c].

[a]*Mohammed VI Polytechnic University (UM6P), Morocco, Center for Remote Sensing Applications (CRSA).*

[b]*ProcEDE, Département de Physique Appliquée, Faculté des Sciences et Techniques, Université Cadi Ayyad, Marrakech, Maroc.*

[c]*Centre d'Etudes Spatiales de la Biosphère (CESBIO), Université de Toulouse, CNES, CNRS, IRD, UPS, Toulouse, France.*

Corresponding author*: Dr. Amazirh Abdelhakim

Email: abdelhakim.amazirh@um6p.ma/ abdelhakim.amazirh@gmail.com

Center for Remote Sensing Applications (CRSA), Mohammed VI Polytechnic University (UM6P), Hay Moulay Rachid-Benguerir, Morocco.

Abstract

Accurate estimation of evapotranspiration (ET) is of crucial importance in water science and hydrological process understanding especially in semi-arid/arid areas since ET represents more than 85% of the total water budget. FAO-56 is one of the widely used formulations to estimate the actual crop evapotranspiration ($ET_{c\ act}$) due to its operational nature and since it represents a reasonable compromise between simplicity and accuracy. In this vein, the objective of this paper was to examine the possibility of improving $ET_{c\ act}$ estimates through remote sensing data assimilation. For this purpose, remotely sensed soil moisture (SM) and Land surface temperature (LST) data were simultaneously assimilated into FAO-dualK_c. Surface SM observations were assimilated into the soil evaporation (E_s) component through the soil evaporation coefficient, and LST data were assimilated into the actual crop transpiration ($T_{c\ act}$) component through the crop stress coefficient. The LST data were used to estimate the water stress coefficient (K_s) as a proxy of LST (LST_{proxy}). The FAO-Ks was corrected by assimilating LST_{proxy} derived from Landsat data based on the variances of predicted errors on K_s estimates from FAO-56 model and thermal-derived K_s. The proposed approach was tested over a semi-arid area in Morocco using first, *in situ* data collected during 2002-2003 and 2015-2016 wheat growth seasons over two different fields and then, remotely sensed data derived from disaggregated Soil Moisture Active Passive (SMAP) SM and Landsat-LST sensors were used. Assimilating SM data leads to an improvement of the $ET_{c\ act}$ model prediction: the root mean square error (RMSE) decreased from 0.98 to 0.65 mm/day compared to the classical FAO-dualK_c using *in situ* SM. Moreover, assimilating both *in situ* SM and LST data provided more accurate results with a RMSE error of 0.55 mm/day. By using SMAP-based SM and Landsat-LST, results also improved in comparison with standard FAO and reached a RMSE of 0.73 mm/day against eddy-covariance $ET_{c\ act}$ measurements.

Key words: Evapotranspiration; Data assimilation; FAO-dualK_c; Soil moisture; Land surface temperature.

1. Introduction

Accurate estimation of surface evapotranspiration (ET) is crucial to understand land-surface interaction processes. Additionally, ET is the dominant factor in the water cycle, especially in arid and semi-arid regions. About 85 to 90 % of precipitation returns to the atmosphere through ET (Rosenberg et al., 1983). Moreover, ET estimates have an important role in monitoring drought (Bhattarai et al., 2019; Gerhards et al., 2019) and other extreme climatic events (Littell

et al., 2016; Molden et al., 2010), as well as water resource management (Madugundu et al., 2017; Tasumi, 2019). In this case the objective is to have accurate ET estimates that allow computing irrigation requirements. Precise actual crop evapotranspiration ($ET_{c\ act}$) estimates are the key for the quantification of crop water requirements, which allow the optimization of irrigation especially in semi-arid and arid areas that suffer from a pronounced shortage of water (Allen et al., 2011; French et al., 2015). Several techniques were developed and used to monitor $ET_{c\ act}$ at different space-time scales. At plot or field scale, we found the eddy correlation system (Allen et al., 2011; Baldocchi et al., 1988), while at a larger scale, the scintillometer can provide $ET_{c\ act}$ over a transect up to 5 km (Ezzahar and Chehbouni, 2009; Kohsiek et al., 2002). Other approaches for measuring $ET_{c\ act}$ were discussed in Alfieri et al. (2018) and Er-Raki et al. (2013).

Concerning $ET_{c\ act}$ predictions, several models with different degrees of complexity have been developed during the past 30 years (Li et al., 2009; Seguin and Itier, 1983). Note that,crop ET (ET_c) refer to optimal, well-watered conditions and pristine cultivated crops, i.e. cropped in conditions without any stress conditions and may be estimated with models while under field conditions actual ET is estimated with models because crops are generally subject to water (and/or other stress conditions). Some of these models use remotely sensed data such as surface albedo, Leaf Area Index (LAI), Normalized Difference Vegetation Index (NDVI), Land Surface Temperature (LST) (Allen et al., 2011; Granger, 2000; Kharrou et al., 2013; Kustas and Norman, 1996; Li et al., 2009) and soil moisture (Elfarkh et al., 2021; Gokmen et al., 2012; Walker et al., 2019). $ET_{c\ act}$ component can be predicted based on water balance at a daily time scale. Among this family of models, the FAO dual crop coefficient model (FAO-dualK_c, Allen et al., 1998) is the most common and operational model to retrieve $ET_{c\ act}$, which was extensively used for modeling water consumption and growth of plants (e.g., Alberto et al., 2014; Barker et al., 2018; Ko et al., 2009; Liu and Luo, 2010). The SIMDualKc software (Paço et al., 2014; Paredes et al., 2014; Pereira et al., 2020; Rosa et al., 2012b, 2012a) was set up based on FAO-dualKc to simulate $ET_{c\ act}$ and its components. In contrast with other models based on energy balance theory, the FAO-56 model requires limited input parameters. Several studies used the FAO model to retrieve $ET_{c\ act}$ over various crop types where wheat is the most studied crop among small grain cereals (e.g. Amazirh et al., 2021; Drerup et al., 2017; French et al., 2020; Rafi et al., 2019). Recently, Pereira et al. (2021) provides a review of the studies using the FAO-dualKc over wheat and other crop types. The FAO-dualK_c approach allows for the partitioning of $ET_{c\ act}$ into soil evaporation (E_s) and plant transpiration ($T_{c\ act}$) by separating

the crop coefficients ($K_{c\ act}$) into a basal crop ($K_{cb\ act}$) and soil evaporation (K_e) coefficients. Despite the operationality of the FAO-dualK_c, several studies stated that FAO-dualK_c tends to under/overestimate soil evaporation (E_s) at the beginning or the end of the season when the surface is under bare soil conditions (Amazirh et al., 2021; Boulet et al., 2019; Olivera-Guerra et al., 2018). In this context, many papers deal with the use of soil moisture (SM) data to retrieve soil evaporation under bare soil conditions (Amazirh et al., 2018; Zribi et al., 2011). Moreover, the crop $T_{c\ act}$ estimates is based on the root zone water balance reflecting the variation of the root zone soil moisture (RZSM). Therefore, using RZSM measurements will improve the $T_{c\ act}$ estimates. The root zone soil moisture is a state variable that is quite difficult to estimate from meteorological data alone or remote sensing data. For this reason, as an attempt to improve $ET_{c\ act}$ estimates, Kalma et al. (2008) and Li et al. (2009) used LST data to estimate water stress indices. More recently, LST data were used to retrieve the stress coefficient (K_s) used by the FAO approach (DeJonge et al., 2015; Ihuoma and Madramootoo, 2017; Kullberg et al., 2017).

Other techniques attempt to combine complementary information from hydrological models and observed data for mapping $ET_{c\ act}$. This technique is named data assimilation (Kumar et al., 2008; McLaughlin et al., 2006). The data assimilation technique is based on minimizing the mismatch between the model outputs and observations, by making the optimal use of all available information. We distinguish between two categories of data assimilation schemes: sequential assimilation like Ensemble Kalman Filter and optimal interpolation. The former technique has been widely used in hydrology (Chen et al., 2013; Moradkhani et al., 2005; Wang et al., 2009; Xie and Zhang, 2010). The latter is variational assimilation (e.g., 4-dimensional variational assimilation (Caparrini et al., 2004; Courtier et al., 1993)). Several research works used data assimilation techniques to estimate $ET_{c\ act}$ at different levels (Er-Raki et al., 2008; Merlin et al., 2006; Neale et al., 2012; Pipunic et al., 2008). Recently, many research works used the variational data assimilation technique to update and improve the $ET_{c\ act}$ estimates and its components (e.g. Abdolghafoorian and Farhadi, 2020; Tajfar et al., 2020; Xu et al., 2019, 2016). For the sequential data assimilation technique, Kalman Filter (KF) and its variants are the widely used techniques for the $ET_{c\ act}$ retrieval due to their simple conceptual formulation and relative ease of implementation compared to other techniques (Bateni and Entekhabi, 2012; Er-Raki et al., 2008; He et al., 2019; Xu et al., 2011). KF provides a sequential, unbiased, and minimum error variance estimate under the assumption of known statistics of system and measurement errors for a linear problem. The KF provided a comparable result with other popular assimilation methods, despite its simple conceptual formulation which did not require

any integrations backward in time compared to other variational assimilation techniques (4DVAR, 3DVAR…). However, KF does not account for nonlinearities in hydrological systems, for this, a variant of KF (e.g. extended Kalman filters) could solve some nonlinear problems. Even that, KF affords very good results compared to other complicated models such as the variational method (Tian et al., 2008). In addition, KF requires few restrictive assumptions which make it operational. Therefore, KF seems to be suitable for hydrological linear problems such as modeling $ET_{c\ act}$. Data assimilation technique seems to be a promising tool to improve the $ET_{c\ act}$ estimates when combining with FAO model. Er-raki et al. (2008) have shown that assimilating LST data into FAO-56 single crop model improves the overall $ET_{c\ act}$ estimates. Er-raki et al. (2008) in their paper reach a satisfactory result after assimilating LST data in FAO single crop coefficient with RMSE values dropping down from 0.69 to 0.46 mm/day compared to open-loop FAO, which corresponds to an improvement of 40% when assimilating LST into the FAO56 approach. In the same vein, the objective of this paper is to use data assimilation in conjunction with FAO-dualK_c methods to improve $ET_{c\ act}$ estimates. We first assimilate time domain reflectometry (TDR) near-surface SM (0-5cm) observations into FAO-dualK_c to improve the soil E_s estimates. Then, TDR-SM and infrared thermal radiometer (IRT) derived LST data were jointly assimilated to improve soil E_s and wheat crop $T_{c\ act}$, respectively. A sequential assimilation scheme was applied to update the E_s and $T_{c\ act}$ estimates. Secondly, Landsat 7/8 derived-LST and disaggregated Soil Moisture Active Passive (SMAP)-SM data at 100 m resolution were used in conjunction with a sequential assimilation approach over two wheat fields named B123 and F16 near Marrakech city in central Morocco.

2. Sites and data description

2.1. Sites description

The present work was conducted over the Tensift region in central Morocco (Figure 1). This area is known as a semi-arid area with low and irregular precipitation against high potential ET_o. Numerous studies have been performed in this region since 2002-2003 to address various problems regarding the use of water, understanding the integrated hydrological functioning of the Tensift semi-arid basin, as well as improving our knowledge of fundamental hydrological processes (Amazirh et al., 2017; Chehbouni et al., 2008; Merlin et al., 2018). The Tensift basin receiving about 250 mm/year of rainfall, while the reference evapotranspiration (ET_o) is about 1600 mm/year, according to the FAO-56 model (Allen et al., 1998). Two study fields have been

monitored during 2002-2003 and 2015-2016 wheat agricultural seasons named by B123 and F16, respectively. Both fields were irrigated by flood gravitation irrigation systems. Flowmeters were used to collect precisely the irrigation volumes of the two irrigated fields. Irrigation was applied every 1 to 3 weeks from December 2015 to April 2016 during the 2015–2016 season. The 4 ha F16 field was irrigated 8 times with a volume of 64 mm each, while the B123 field was irrigated 4 times with a volume of 24 mm each. These fields are located in an irrigated perimeter named by R3 situated about 40 km east of the city of Marrakech (31°40′9.46″N, 7°35′45.64″W). The B123 and F16 fields occupied an area of approximately 4 ha each (0.85 km * 4.15 km) involving 7 pixels. The surrounding two fields were also cultivated with wheat crops and were similar to the same irrigation system. Both fields were known for high clay contents (47%) and 18% of sand fraction. The sowing dates were the 13th December 2015 and 14th January 2003 for the F16 and B123 irrigated sites, respectively (Amazirh et al., 2017; Olivera-Guerra et al., 2018).

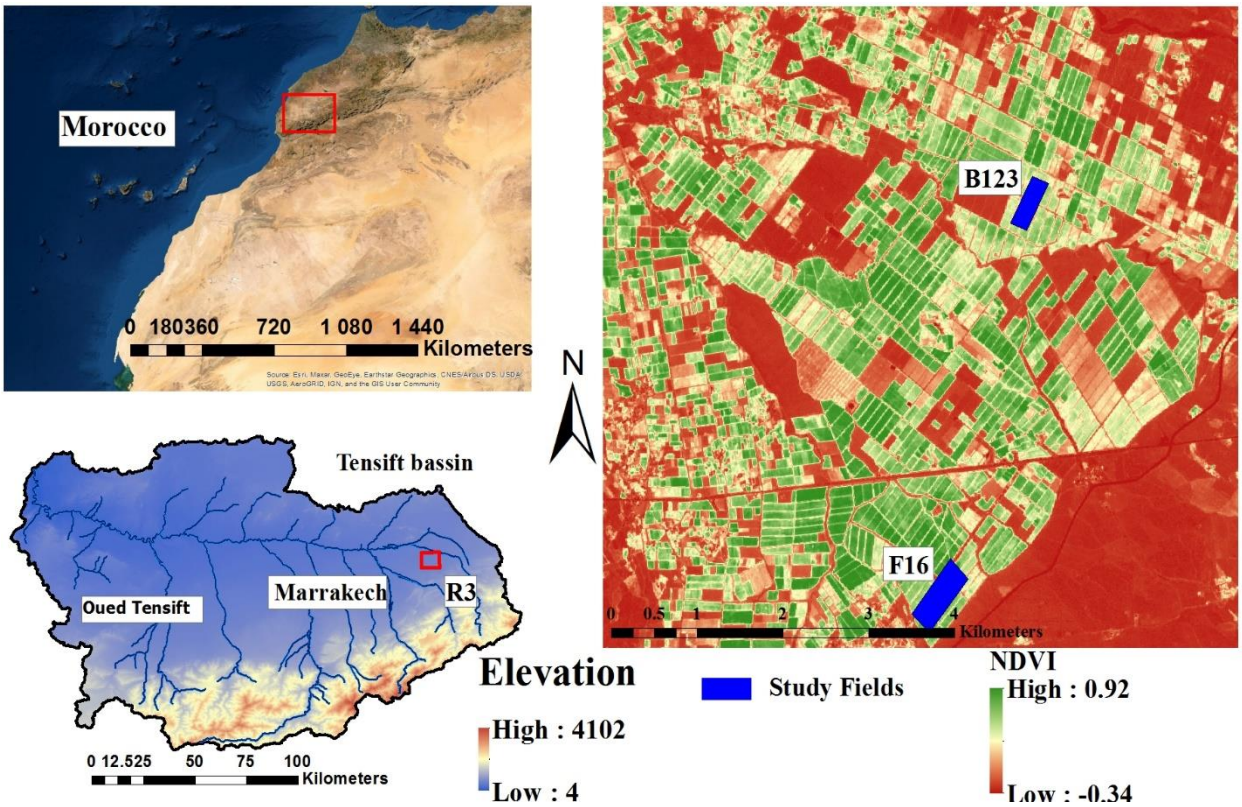

Figure 1: Location of the study area R3 (red rectangle). Study fields are illustrated with blue rectangles.

2.2. Experimental data set

2.2.1. Weather station

During the investigated agricultural seasons, an experiment has been set up for each site. An automatic weather station was set up, over an alfalfa cover near the studied wheat fields, to provide continuous climatological data at a sub-hourly time step, including air temperature (T_a, HMP60, Vaisala, Oyj, Helsinki, Finland), relative humidity (rh_a, HMP60, Vaisala, Oyj, Helsinki, Finland), solar radiation (R_g, pyranometer, LI-COR LI-200X, Lincoln, NE, USA), wind velocity (u_a, anemometer, R.M. Young 3002, Traverse City, USA) and precipitation (P, automatic rain gauge, Texas Electronics TE525 MM, USA). Reference evapotranspiration (ET_0) was calculated on a daily basis using the Penman-Monteith equation for short canopies (Allen et al., 1998).

2.2.2. Eddy covariance stations

Each field was equipped with an eddy covariance station (EC) consisting of a 3D sonic anemometer (CSAT3, Campbell Scientific Ltd. Logan, UT, USA) that measures the three components of wind speed and a Krypton hygrometer (KH21, Campbell Scientific Ltd. Logan, UT), providing continuous measurements of energy fluxes, vertical sensible heat (H_{obs}) and latent heat (LE_{obs}) fluxes which is equivalent to $ET_{c\ act\ obs}$. The net radiometer (Kipp and Zonen CNR4, Campbell Sci, Delft, The Netherlands) measured the surface net radiation (R_n) at 2.6 m height and the soil heat flux (G) was measured at 5 cm depth by using two heat flux plates (HPF01, Campbell Sci, Logan, USA) over the wheat crop fields. An average output of the two plates was used. The two plates were buried with thermocouples at two depths to account for heat storage. Note that, the EC systems were installed at a height of 2.6 m, and the maximum height of wheat was 0.74 m and 0.90 m for B123 (2002-2003) and F16 (2015-2016) sites, respectively. Therefore, the EC system was at least 1.70 m above the canopy. The choice of the installation height actually resulted in a compromise between two constraints: 1) sampling within the field for a range of wind directions and 2) measuring above the roughness layer all along the agricultural season. The relative height of 1.70 m above the canopy ensures that the EC is in the constant flux layer, which is located approximately 1.5-2 canopy heights above the soil surface (Burba, 2013). The two energy fluxes were extracted from KH21 hygrometer measurements, which quantify the fluctuations of atmospheric water vapor and temperature. The collected raw EC data at 20 Hz are processed in the laboratory using the EC-pack software developed by the Meteorology and Air Quality Group, Wageningen University (available for download at http://www.met.wau.nl/). The flux tower $ET_{c\ act}$ is calculated as a multiplication of the air density by the fluctuation of the mean density of water vapor in the air, the fluctuation of the mean vertical wind velocity, and the latent heat of vaporization. Before using such an

energy flux data set, a verification of the reliability and the quality of these measurements is needed. The energy balance closure is a way to assess that, by comparing the surface available energy (R_n-G) to the sum of turbulent fluxes (H_{obs}+ LE_{obs}). For the F16 field, the energy budget closure was achieved in Amazirh et al. (2017). The ratio of the turbulent energy flux to available energy (EBR) was 78%, with a strong coefficient of determination (R^2=0.91), while for B123 field, the EBR is equal to 80% with an R^2 equal to 0.92 (Er-Raki et al., 2011). The slope of the regression forced through the origin was about 1.30 and 1.22 for F16 and B123 fields, respectively. The closure error is close to 10 % for both field which is in the acceptable ranges (from 10% to 30%) reported in Twine et al. (2000). The obtained results are relatively good and the closure of the energy balance is relatively well verified in comparison with other studies (Elfarkh et al., 2021; Testi et al., 2004; Twine et al., 2000). To correct some small uncertainties of non-closure of the energy balance, the Bowen ratio was used to recompute H and LE by forcing the energy balance closure with the measured values of Bowen ratio. The observed data were carefully processed and rigorously screened, some gaps were observed in the collected data, these data were excluded.

2.2.3. In situ soil moisture and land surface temperature measurements

Soil moisture data were also collected over both sites at different depths (5, 10, 20, 30, 50, 70 cm), at a half-hourly time step, using time-domain reflectometer (TDR) probes buried under the eddy covariance system for each field. Only one point was selected under the eddy covariance stations for each field. This is due to fact that the fields are irrigated with flooding system which implies a homogeneous fraction of wetted areas, where all the pixels have the same percentage of irrigation water, which means uniform soil moisture within the site. Also, the wheat crop covers the field uniformly (uniform distribution of seeds), which means that the shaded area within the field is uniform. This homogeneity all over the field could explain the use of one location instead of several locations. Note that, SM was measured up to 0.7 m, but only data from 0.05 to 0.5 m were used in this study. This is due to, the measured rooting depths which are 0.52 and 0.50 m for F16 and B123 fields (Er-Raki et al., 2007). The collected SM data were calibrated using the gravimetric technique by taking soil samples at each depth. SM at the surface was used in this study to improve soil E_s through assimilation technic.

In addition, brightness surface temperature (T_{bs}) was measured by an Apogee 8–14 μm thermal radiometer sensor (SI-121, Apogee IRTS-P's, Inc., Logan, Utah, USA) in each field, set up at a 2 m height looking at nadir. The T_{bs} is corrected from sensor errors using the sensor body

temperature, then was converted to surface temperature as in Tardy et al. (2016), using the approach proposed by Olioso (1995). The thermal data were corrected from atmospheric effects using the spectral atmospheric transmission and the atmospheric downwelling and upwelling radiances. The atmospheric parameters are obtained from an atmospheric radiative transfer model (MODTRAN, Berk et al., 2005). Finally, LST was estimated by inverting the simplified Plank's law. The derived spectral atmospheric parameters and the surface emissivity permit the conversion of the at-sensor radiance into the top of canopy radiance exempt from atmospheric effects. The corrected temperature was used to improve $T_{c\ act}$ by updating the stress coefficient (K_s).

2.3. Remote sensing data

In this work, Landsat-7 (L7) and Landsat-8 (L8) data were used to provide land surface temperature (LST) while SMAP data were used to extract surface soil moisture (SM) Table (1). Only data over the F16 field were derived because SMAP sensor was launched in 2015 and B123 field was set in 2002.

2.3.1. Landsat data

L7 ETM+ and L8 OLI-TIRS were used in this study. The surface reflectance and thermal radiance (TIR) were downloaded from the USGS website (https://earthexplorer.usgs.gov/). L7 provides one thermal band (band 6) while the L8 provides two thermal bands (bands 10 and 11) but only band 11 was considered which is recommended to be used regarding the quality. TIR data were freely acquired with a spatial resolution of 60 and 100 m for L7 and L8, respectively. The revisit time for each sensor is 16 days with an 8-day offset between the two overpasses, which offers TIR data every 8 days. 13 cloud-free images were collected in the 2015-2016 agricultural season over F16 study field. As mentioned in section 2.1, the F16 field occupied an area of approximately 4 ha (0.85 km × 4.15 km) involving 7 pixels. However, a selection of the pixel where the eddy covariance system was installed has been performed to overcome the edge problem, which can involve the pixels of the surrounded fields. Even if an average over the field was made, it would not impact the results because the surrounding fields are also cultivated with wheat crop with the same irrigation system (gravity) and at the same time.

L7 and L8 have different resolutions, a rescaling approach is needed. Since the spatial resolution of L7 thermal data (60 m) is much finer than spatial resolution of L8 thermal data (100 m), the 60 m TIR data were resampled linearly to 100 m resolution which is the lowest spatial resolution between L7 and L8. The 13 TIR data were then preprocessed to extract the LST. TIR data were

converted to LST data after applying atmospheric correction and correction of surface emissivity. The followed steps are described in Tardy et al. (2016) and the same processing chain was used in Amazirh et al. (2019, 2018). The different correction steps defined in Tardy et al. (2016) allow converting the Landsat digital number to top of atmosphere radiance to top of canopy radiance then, to the physical LST at the surface. An atmospheric correction of the thermal infrared bands' data was firstly carried out using the MODTRAN atmospheric radiative transfer model software. The atmospheric profile composition (vertical air temperature and water content) needed as input to the model has been obtained from the ECMWF European Reanalysis (ERA) Interim product (Dee et al., 2011). As the second step, the at-sensor radiance was converted into surface radiance using the estimated surface emissivity. Then the LST was obtained by inverting Plank's law.

2.3.2. SMAP

SMAP mission was launched in January 2015. This satellite was launched by the National Aeronautics and Space Administration (NASA) with an L-band passive sensor onboard (Entekhabi et al., 2014). SMAP satellite (Entekhabi et al., 2014) is the first L-band mission that combines both radiometer (passive) and radar (active) data dedicated to the study of soil moisture at a range of resolutions from 3 km (active) to 36 km (passive) with a revisit cycle of 2–3 days. It orbits at an altitude of 658 km and provides SM from both descending and ascending overpasses. Despite the high frequency of SMAP data acquisition, the spatial resolution is very low which limits their application, especially to agricultural fields. To fill the gap, many disaggregation methodologies were developed to provide SM at high spatial resolution (Abbaszadeh et al., 2019; Peng et al., 2017). Ojha et al. (2019) used DISPATCH (DISaggregation based on Physical And Theoretical scale Change) method to disaggregate 36 km-SMAP SM resolution to 100 m resolution. All the followed disaggregation steps were described in Ojha et al. (2019). Three steps were followed to downscale the 36 km SMAP SM to 100 m. The 36 km SM is first disaggregated to 1 km resolution using MODIS LST and NDVI (DISPATCH-1 km). The 1 km resolution disaggregated data is next aggregated to the intermediate spatial resolution, and then further disaggregated to 100 m resolution using Landsat-derived LST and NDVI (DISPATCH-100 m). The disaggregation approaches are based on thermal-derived soil evaporative efficiency (SEE) which is a normalization of LST data by its maximum and minimum values derived from the energy balance model. The disaggregated $SM_{DISPATCH}$ products were evaluated over 22 irrigated fields in the same used area. The *in situ* SM measurements have been collected and calibrated as in Amazirh et al.

(2018) during the 2015–2016 season. The disaggregation procedure was tested on 7 dates at Landsat overpass against *in situ* SM. The evaluation of disaggregated SM was done based on statistical results in terms of the correlation coefficient (R), the slope of the linear regression, absolute mean bias, and root mean square difference (RMSD). The results show good results in terms of R which is ranged between 0.6 and 0.9 with a relatively low absolute bias lower than 0.03 m^3/m^3. This approach developed by Ojha et al. (2019), was applied during this work to 36 km-SMAP resolution data products, and the disaggregated data set was used in this study. In this study, only 9 available dates were selected on the Landsat overpass, due to *in situ* data gaps. Another issue is that the evaluation was assessed from December 27, 2015 to January June 01, 2016 (winter wheat growth season) which limit the number of satellite overpasses. In addition, the disaggregated SM products include data gaps, which on some dates unfortunately covered the wheat site.

Table 1 lists the characteristics and the selected dates of L7/8 and SMAP overpasses used in this work.

Table 1: Technical characteristics of satellite products and the selected dates collected in clear sky conditions over the study site.

Sensors /Mission	**Acquisition Time**	**Bands**	**Spatial resolution (m)**	**Temporal resolution (Day)**	**Acquisition date of used data (2016)**
Soil Moisture Active Passive (SMAP)	06:00 AM/PM	Brightness temperature	36 km*	2-3	14, 22, 30 January 02, 10 March 03, 27 April 13, 29 May
Landsat 7 and Landsat 8 (L7/L8)	~11:30 AM	- VNIR⁺ (L7: B3 & B4; L8: B4 & B5) - TIR (B6 for L7 and B10 et B11 for L8)	60 m and 100 for TIR˟ 15 m for VNIR	8	06, 14, 22, 30 January 07, 23 February 02, 10, 18 March 03, 27 April 21, 29 May

* *SMAP data were disaggregated from 36 km to 100 m resolution.*

⁺ *VNIR stands for Visible-near infrared.* ˟ *TIR stands for Thermal infrared. B stands for Band.*

3. Methodologies

3.1. FAO-56: Dual crop coefficient

FAO-56 (Allen et al., 1998) was extensively used to retrieve ET and irrigation scheduling. This is due to its operationality and its simplicity of implementation. The FAO dual crop coefficient (FAO-dualK_c) comes to improve the ET estimates by partitioning ET into soil E_s and plant T_c using reduction evaporation coefficient (K_e) and basal crop coefficient (K_{cb}), respectively, from standard evapotranspiration (ET_0). Under well-watered condition ET_c is written as:

$$ET_c = (K_{cb} + K_e)ET_0 \quad (1)$$

ET_0 being the ET rate over a well-watered crop land covered by a short green, grass-like crop (reference ET), depending only on atmospheric conditions (ASCE-EWRI, 2004). Equation (1) depends only on atmospheric conditions and is adapted to non-hydric stressed crops (standard conditions). To take into account the crop water stress and to catch the real ET ($ET_{c\,act}$), a water stress coefficient (K_s) was introduced into Equation (1) and it becomes:

$$ET_{c\,act} = ET_{FAO} = K_{cb}K_sET_0 + K_eET_0 = T_{c\,act} + E_s \quad (2)$$

Where $ET_{c\,act} \equiv ET_{FAO}$ is the actual crop evapotranspiration under non-standard conditions. K_{cb}, K_e, and K_s are basal crop $T_{c\,act}$ coefficient under non-standard conditions, soil evaporation, and water stress coefficients, respectively.

The K_{cb} values are defined for each crop growth stage. The wheat growth stages are distinct by their lengths (initial (L_{ini}), development (L_{dev}), mid-season (L_{mid}), and late (L_{late})). Lengths of growth stages are usually calculated based on the fractional vegetation cover (f_c) derived from normalized difference vegetation index (NDVI) as in Er-raki et al. (2008), Er-Raki et al. (2007), Olivera-Guerra et al. (2018) and Rafi et al. (2019). During the initial stage, K_{cb} named $K_{cb\,ini}$, mid-season named $K_{cb\,mid}$, and at the end of the growing season, K_{cb} named $K_{cb\,end}$ where the values were taken from Allen et al. (1998). Local calibration of the FAO model has been stressed in this work, by adjusting the default values of lengths of growth stages reported in FAO based on the different equations provided in FAO-56 for adjusting the K_{cb} values. Lengths of growth stages significantly differ from the FAO-56 default values, especially for the duration of phenological phases. However, the calibrated lengths of growth stages were in accordance with the NDVI measurements carried out on the site. Note that, the lengths of the growth stage reported in FAO-56 are informative values which can only be used in locations with no data. Also, the stages durations are changing from one year to another due to its dependence on the

thermal accumulation. The K_{cb} parameter was decomposed into $K_{cb\ ini}$, $K_{cb\ mid}$, and $K_{cb\ end}$. The $K_{cb\ dev}$ is the K_{cb} during the development stage and is estimated using linear interpolation between $K_{cb\ ini}$, and $K_{cb\ mid}$. The K_{cb} was interpolated at the daily scale between the start and end value ($K_{cb\ ini}$, $K_{cb\ mid}$, $K_{cb\ end}$) of each phenological phase as in the FAO-56 documentation. K_{cb} values were adjusted in each growing stage using climatic data. K_e is the evaporation coefficient which is calculated as:

$$K_e = \min\{[K_r(K_{c\,max} - K_{cb})], [f_{ew}K_{c\,max}]\} \quad (3)$$

where $K_{c\ max}$ is the maximum value of crop coefficient (following rain or irrigation), ranged from 1.05 to 1.30 and estimated using meteorological data (Allen et al., 1998). f_{ew} is the fraction of exposed and wetted soil from which most E_s occurs. It is calculated as a function of fraction cover derived from NDVI as suggested by Er-raki et al. (2007). K_r is the reduction coefficient of evaporation. This coefficient depends on the amount of water that can be depleted by E_s during a complete drying cycle (TEW) and the cumulative depth of water depleted at the end of day i-1 ($D_{e,i-1}$). It is calculated as:

$$K_{r,FAO} = \frac{TEW - D_{e,i-1}}{TEW - REW} \quad ; D_{e,i-1} > REW \quad (4)$$

$$K_{r,FAO} = 1 \quad ; D_{e,i-1} < REW$$

where REW is the readily evaporated water, which is the maximum depth of water that can be easily evaporated without restriction. REW (mm) depends on soil properties. FAO provides REW value for each soil texture (Allen et al., 1998) ranging from 5 to 12 mm. To estimate the maximum amount of water that can be evaporated (TEW), the top layer depth that can be evaporated (Z_e), the soil moisture at field capacity (SM_{FC}), and the soil moisture at wilting point (SM_{WP}) are required. TEW is calculated as:

$$TEW = 1000(SM_{FC} - 0.5SM_{WP})Z_e \quad (5)$$

SM_{FC} and SM_{WP} are reported for each soil texture classification in FAO-56.

A daily water balance is required to estimate the cumulative depth of E_s (depletion) from the soil surface layer (D_e). A simplification of the water balance equation was established, where runoff flux is ignored when working on a flat area.

$$D_{e,i} = D_{e,i-1} - P_i - \left(\frac{I_i}{f_w}\right) + \frac{E_{s,i}}{f_{ew}} + DP_{e,i} \quad (6)$$

where P_i is precipitation input (mm) on day i and I_i is irrigation measured for each site (mm) on day i, $E_{s,i}$ is soil evaporation (mm) on day i, calculated as $Ke \times ET_0$ (Allen et al., 1998; Bos et al., 2008) and f_w is the fraction of soil surface wetted by irrigation. In case of irrigation event or precipitation more than 3 mm/day, f_w is taken equal to 1, otherwise, f_w is set to zero. In this study, fields are irrigated by flood-irrigation technique, therefore, f_w set to 1 during irrigation event. The $DP_{e,i}$ is deep percolation loss (downward drainage) from the topsoil layer on day i (mm). Deep percolation occurs when soil moisture exceeds field capacity following heavy rain or irrigation. The $DP_{e,i}$ equation assumes that water content is at field capacity so that $D_{e,i}$ set to zero and the E_s process switch off on the day of a complete wetting event. From equation (6), $DP_{e,i}$ then is calculated as follow:

$$DP_{e,i} = P_i + \left(\frac{I_i}{f_w}\right) - D_{e,i-1} \quad (7)$$

The procedure to estimate the transpiration reduction factor K_s [0-1] is similar to K_r. K_s is calculated based on a daily computation of the water balance for the root-zone layer Z_r (m) which is written as follow:

$$K_{s,FAO} = \frac{TAW - D_r}{TAW - RAW} = \frac{TAW - D_r}{(1-p)TAW} \quad (8)$$

When D_r > RAW the stress is presumed to start, and K_s is calculated using Equation (8). Conversely, when $D_r \leq$ RAW then K_s is equal to 1.

D_r is the root zone depletion (mm), TAW is total available water in the root zone [mm], RAW is readily available soil water of the root zone (*p**TAW) and *p* is the depletion fraction for no stress which is a fraction of TAW that a crop can extract from the root zone without causing water stress. The TAW is linked to the root depth and to the difference between the water content at field capacity and wilting point as expressed in Equation (9):

$$TAW = 1000(SM_{FC} - SM_{WP})Z_r \quad (9)$$

3.2. Assimilation approaches

Through assimilation, we seek to improve first daily soil E_s by integrating observed and remotely sensed SM, then integrating observed and remotely sensed LST into the $T_{c\ act}$ rate. Figure 2 presents an illustration of how the correction is performed using sequential assimilation to improve state variables using observations to correct the model. The state variables in our case are the soil E_s and the plant $T_{c\ act}$. The used sequential assimilation

approach is based on generating an ensemble of perturbations, to obtain the forecast error covariance information required by the standard Kalman filter update equation.

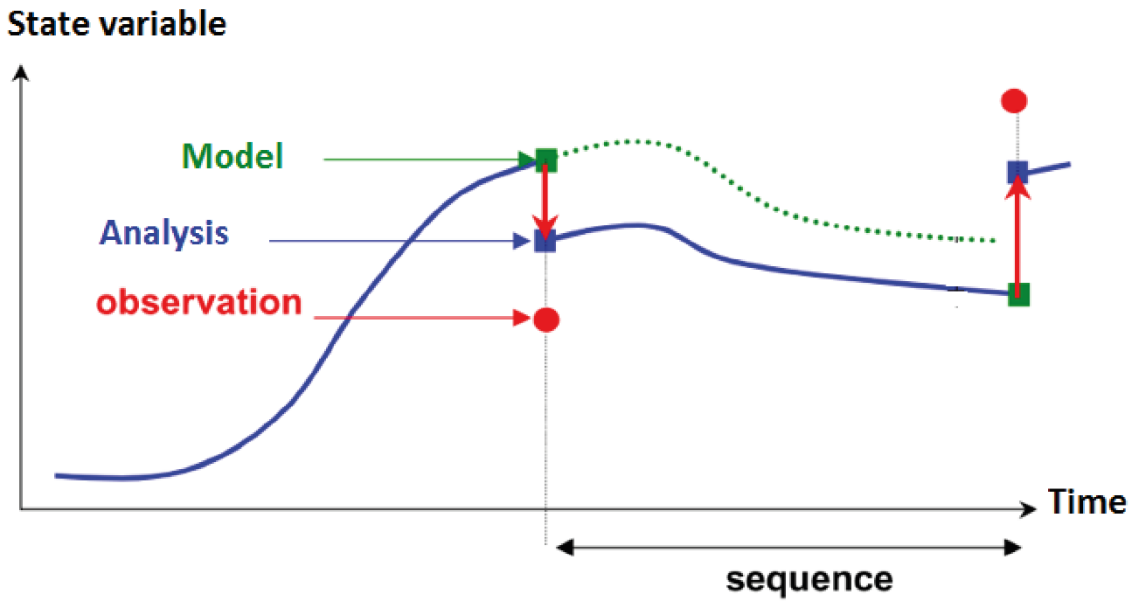

Figure 2: Sequential data assimilation principle to obtain corrected value (analysis) by updating model using observation (Stanev and Schulz-Stellenfleth, 2014).

Two assimilation methods were used, the first one, by assimilating SM into FAO-dualK_c soil E_s component and the second, by assimilating jointly SM and LST into FAO-dualK_c soil E_s and wheat $T_{c\ act}$. Both approaches are detailed below.

3.2.1. Method 1: SM only

As a first step, SM was assimilated into the FAO model to improve the E_s component estimates. The data assimilation scheme is used to correct the depletion depth D_e used by the FAO-dualK_c by using first, *in situ* and then remote sensing SM at field scale integrated into K_e equation. Data assimilation is based on the use of an optimal and simple linear scheme to sequentially assimilate K_e as proposed by Schuurmans et al. (2003) and used by Er-Raki et al. (2008). This method has been chosen due to its simplicity and to keep FAO method operational. The assimilated K_e is written as:

$$K_{e,New} = K_{e,FAO} + \mathbf{K_{evap}}\left(K_{e,SM} - K_{e,FAO}\right) \quad (10)$$

where $\mathbf{K_{evap}}$ is the Kalman gain that minimizes the analyzed error covariance, calculated as:

$$\mathbf{K_{evap}} = \frac{\sigma^2_{Ke,FAO}}{\sigma^2_{Ke,FAO}+\sigma^2_{Ke,SM}} \quad (11)$$

422 $\sigma^2_{Ke,FAO}$ and $\sigma^2_{Ke,SM}$ are the variances of predicted errors on K_e estimates from FAO-dualK_c
423 model and SM observations, respectively.

424 $K_{e,FAO}$ and $K_{e,New}$ are the estimated K_e by the FAO-dualK_c approach before and after data
425 assimilation, respectively. While $K_{e,SM}$ is the K_e estimated from SM observations derived from
426 *in situ* or SMAP disaggregated data. The $K_{e,SM}$ is calculated as Equation (3) except that the D_e
427 equation is forced by SM data instead of using the water balance model at the surface. The D_e
428 equation using SM information is written as follow:

429 $$D_e = 1000(SM_{FC} - SM_{obs})Z_e \quad (12)$$

430 ### 3.2.2. Method 2: Combined assimilation of SM and Land Surface Temperature

431 FAO-dualK_c model is based on water balance model to estimate K_s. In order to improve wheat
432 crop $T_{c\ act}$ estimates, surface temperature can be used to reflect the crop water status by
433 calculating stress index for the root-zone layer. The used assimilation scheme is the same used
434 for assimilating SM (sequential assimilation):

435 $$K_{s,New} = K_{s,FAO} + \mathbf{K_{stress}}(K_{s,LST} - K_{s,FAO}) \quad (13)$$

436 where the $\mathbf{K_{stress}}$ is the Kalman gain calculated as equation:

437 $$\mathbf{K_{stress}} = \frac{\sigma^2_{Ks,FAO}}{\sigma^2_{Ks,FAO} + \sigma^2_{Ks,LST}} \quad (14)$$

438 $K_{s,FAO}$ is the stress coefficient calculated by water balance in the root zone layer, While $K_{s,LST}$
439 is estimated as a proxy of LST, where the LST is normalized by its maximal and minimal values
440 as in Idso et al. (1981).

441 $$K_{s,LST} = LST_{proxy} = \frac{(LST - T_a)_{max} - (LST - T_a)}{(LST - T_a)_{max} - (LST - T_a)_{min}} \quad (15)$$

442 where $LST - T_a$ is the difference between surface temperature and air temperature; $(LST - T_a)_{min}$
443 is the lower limit of $(LST - T_a)$ of a surface which is transpiring at the potential rate, and
444 $(LST - T_a)_{max}$ the expected differential in the case of a non-transpiring crop.

445 An overview of the methodologies using remote sensing data is represented in the flowcharts,
446 Figure 3.

447

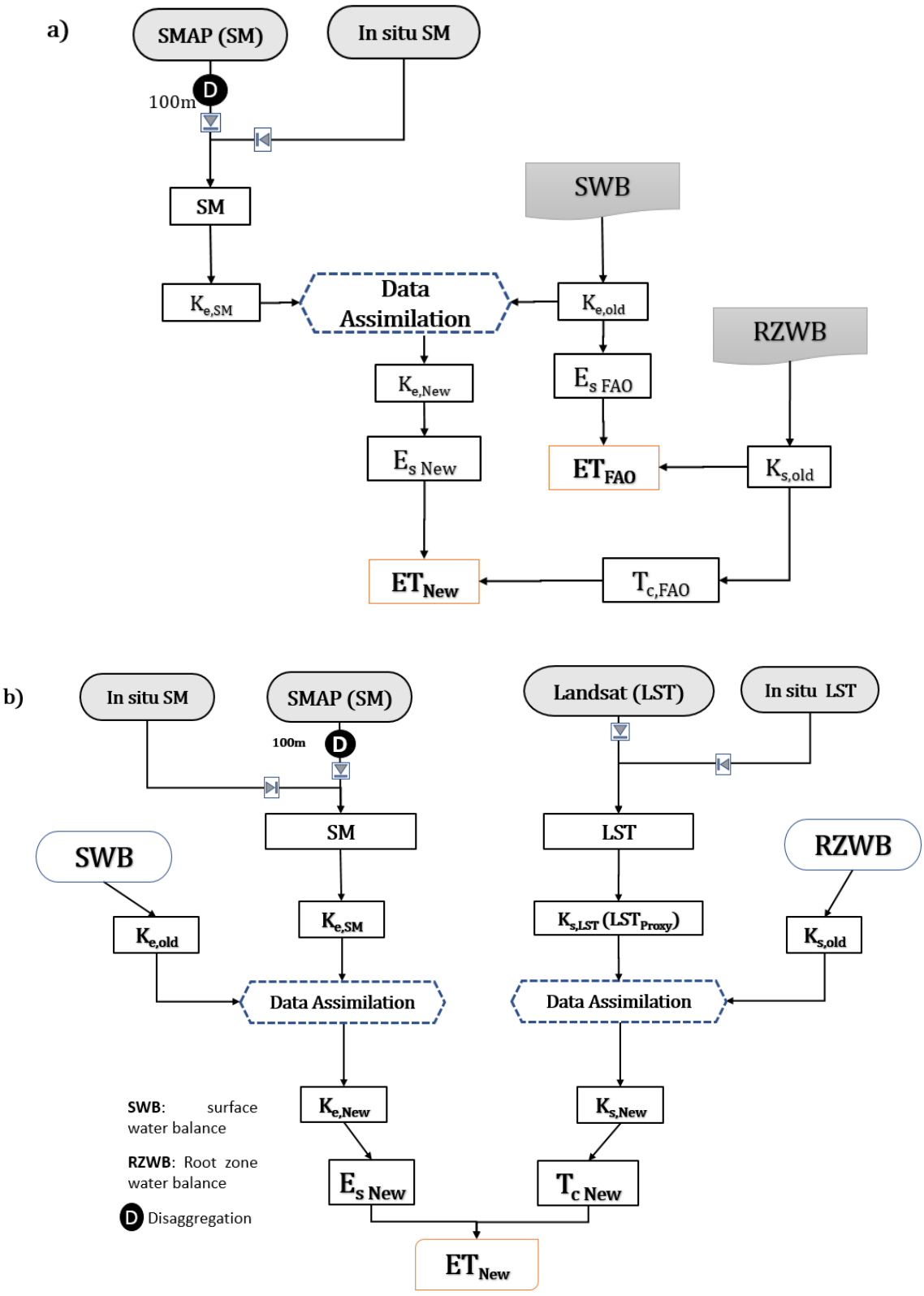

Figure 3: Schematic diagrams presenting an overview of the main inputs, models and outputs of the assimilation of soil moisture into FAO-dualK_c (a) and SM & LST conjointly (b). Standard FAO-dualK_c is also presented in (a).

4. Results and discussions

4.1. Remote sensing data analysis

4.1.1. Landsat against in situ LST

As an important step for investigating the use of LST data for the assimilation approach, it is essential to investigate the relevance between the Landsat LST data and in situ measurements. In this section a comparison between the 100 m Landsat LST and in situ TIR measurements was performed. In Figure 4, Landsat LST is plotted against *in situ* LST data in order to check the reliability of the remote sensed Landsat LST.

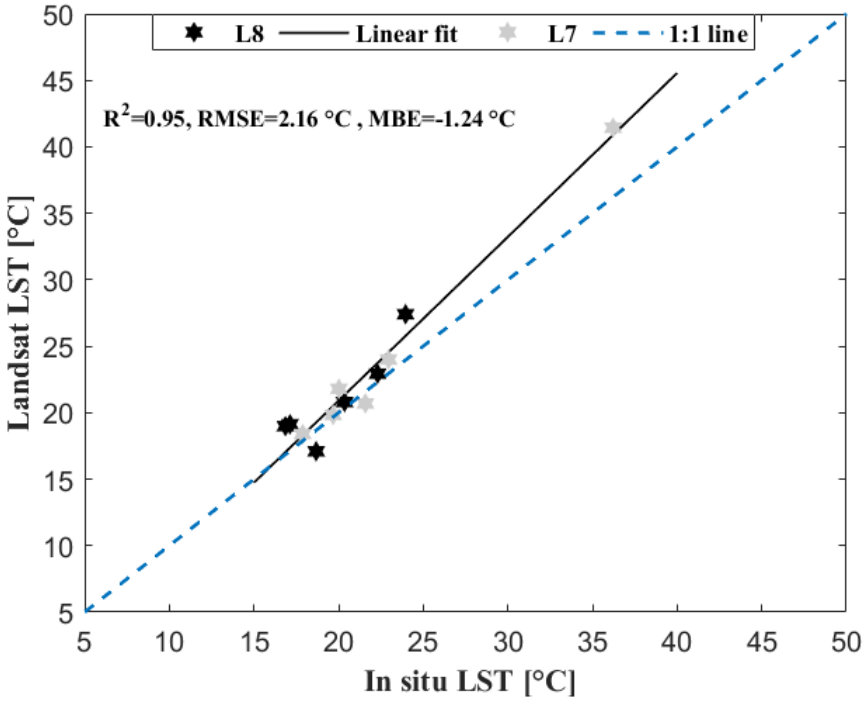

Figure 4: Land surface temperature derived from Landsat-7 (L7) and -8 (L8) versus in situ (In situ LST) measurements for F16 field. Line 1:1 (dotted blue line) and regression line (black solid line) were also presented.

The comparison between both temperatures showed good agreement, with a determination coefficient equal to 0.95 and an error (RMSE) equal to 2.16 °C. The results are slightly consistent with the one obtained in Amazirh et al. (2018), where they found an error close to 3 °C, over a field near the study field, by applying the same algorithm used in this work. Landsat overestimates slightly LST. This is due to the difference in the spatial extent of remotely sensed and *in situ* observations, where the Apogee radiometer was installed at a 2-m height, which limits the spatial representativeness of its measurements. The observed underestimation is quite similar for both L7 and L8 compared to in situ measurements. An RMSE of 2.33 °C and MBE

of -1.30 °C were obtained when comparing L-7 and in situ measurements, while when comparing L8 against in situ LST, an RMSE of 1.98 °C and MBE of -1.18 °C were obtained. This allows, to combine the both satellites to benefit from the temporal resolution of both satellites.

4.1.2. TDR against disaggregated-SMAP soil moisture

Before using the 100 m resolution SMAP disaggregated SM ($SM_{DISPATCH}$), it is important to check their reliability and quality. To this end, an evaluation against *in situ* SM over the F16 study field was performed. The comparison results are illustrated in Figure 5.

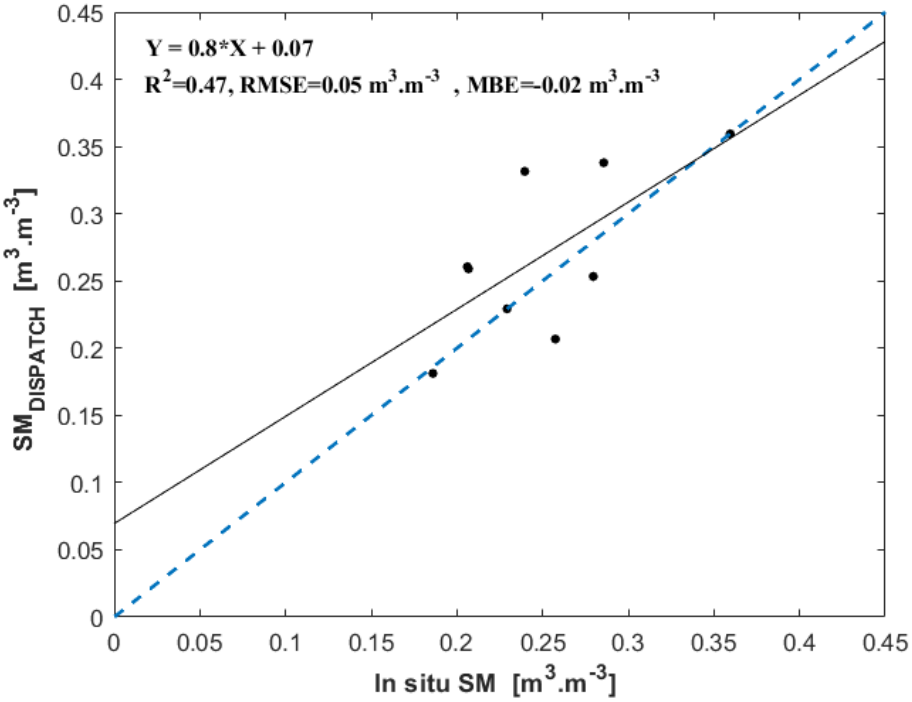

Figure 5: Disaggregated SMAP-soil moisture ($SM_{DISPATCH}$) against in situ soil moisture (In situ SM) over the F16 field. Line 1:1 (dotted blue line) and regression line (black solid line) were also presented.

The comparison results show that $SM_{DISPATCH}$ matches relatively well the TDR *in situ* measurements with a root mean square error (RMSE) of 0.05 $m^3.m^{-3}$ and mean bias error of -0.02 $m^3.m^{-3}$. The regression line is close to the 1:1 line and the determination coefficient is equal to 0.47 which corresponds to Pearson correlation coefficient (R) value equal to 0.69 that lies in the results range [0.5-0.9] reached by Ojha et al. (2019) over the 22 fields in the same area. This result is encouraging despite the acceptable statistics considering the localization of

the *in situ* measurements within the disaggregated SMAP SM pixel. Moreover, another issue that could lead to differences between the disaggregated and *in situ* SM is that the ground SM sensors are buried at a depth of 5 cm, while the penetration of the L-band wave varies between 2 and 5 cm depending on soil conditions (eg. soil texture).

4.2. In situ evaluation of the assimilation approaches

As an assessment of the assimilation methodologies, this procedure was tested over both B123 and F16 sites. *In situ* SM and LST data are available over both sites. The first step was to test the effect of near-surface SM assimilation alone into FAO-dualK_c E_s component. The second step was to assess the performance of coupled assimilation of both SM and LST variables into FAO-dualK_c $ET_{c\ act}$. Assimilating LST alone into the FAO model was also tested over both sites. Results (results not shown) indicate that assimilating LST only, slightly improves the $ET_{c\ act}$ estimations (an error difference of 0.92 mm/day) and an R^2 equal to 0.64 with and an MBE less than 0.57 m/day for the F16 site. The slightly improvement of $ET_{c\ act}$ estimates using LST only is due to the fact that LST data is representing the soil and wheat temperatures and a partition of LST is needed to incorporate LST data into FAO model. Otherwise, assimilating LST data into FAO single approach coefficient could improve the $ET_{c\ act}$ results significantly as found in Er-Raki et al. (2008).

Figure 6 presents the daily temporal comparison of the $ET_{c\ act}$ estimates using the assimilation approaches and the observed $ET_{c\ act}$. The statistical results of the assimilation approaches and the standard FAO-dualK_c are presented in Table 2. The $ET_{c\ act}$ estimates are evaluated by comparing them with the measured $ET_{c\ act}$ by the Eddy covariance system from both wheat sites (B123 and F16). Ground-based SM and LST data are available at a 30 min time scale, which allows us to choose the number of assimilation dates without restrictions. In our case, an 8-day frequency was used, which corresponds to the Landsat revisit time-frequency over our study sites. First only SM data are assimilated (SM-only) then SM and LST couple are assimilated.

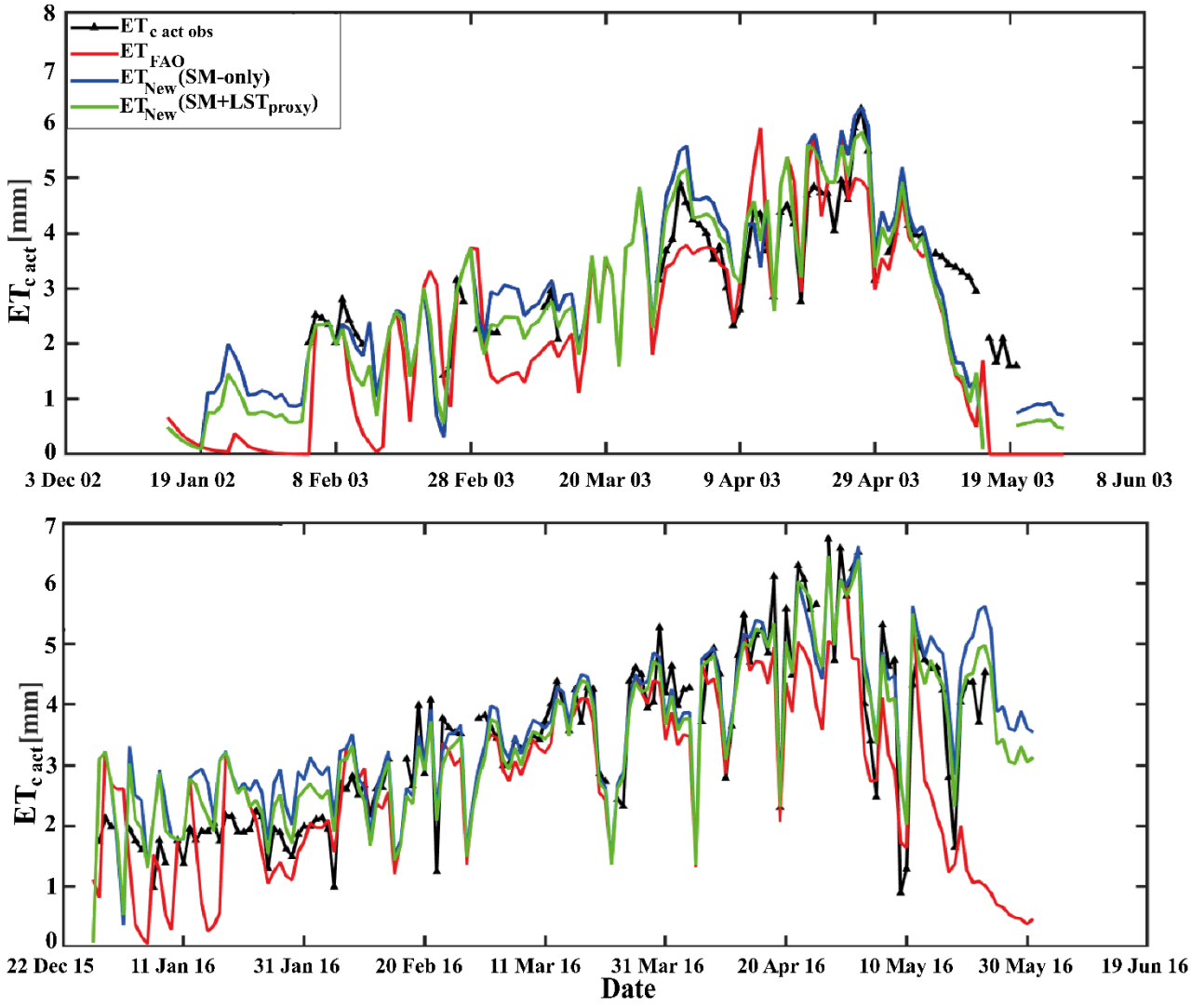

Figure 6: Daily temporal comparison between FAO-dualK_c and observed $ET_{c\ act}$ without assimilation (ET_{FAO}) and when assimilating SM-only and when assimilating SM and LST_{proxy} couple for B123 (top) and F16 (bottom) sites.

Table 2: Statistical analysis of $ET_{c\ act}$ simulated by the FAO-dualK_c before assimilation and after assimilations for both wheat fields.

Statistics	**R^2**		**RMSE (mm/day)**		**MBE (mm/day)**	
Fields	**B123**	**F16**	**B123**	**F16**	**B123**	**F16**
Methods						
ET_{FAO} (no assimilation)	0.72	0.63	1.01	0.98	-0.44	-0.47
SM-only	0.77	0.85	0.73	0.65	-0.14	-0.32
SM+LST_{proxy}	0.77	0.87	0.71	0.55	0.03	-0.14

524 ***NOTE.*** **ET_{FAO} (no assimilation):** open loop FAO model. **SM-only**: assimilating only soil moisture data
525 into FAO model. **$SM+LST_{proxy}$**: Assimilating conjointly soil moisture and Land surface temperature
526 into FAO model.
527 From Table 2 the RMSE between measured and estimated $ET_{c\ act}$ using standard FAO-dualK_c
528 (no assimilation) for the F16 and B123 sites are, 0.98 and 1.01 mm/day, respectively. As seen
529 in Figure 6, without assimilation, standard FAO-dualK_c severely underestimates $ET_{c\ act}$ (see the
530 MBE values in Table 2). The assimilation of surface soil moisture alone is significantly
531 improving the estimate of soil E_s component, which ameliorates $ET_{c\ act}$ estimates at the field
532 scale. Without and with SM assimilation, the RMSE decreases from 0.98 and 1.01 to 0.65
533 mm/day and 0.73 mm/day, and the R^2 increases from 0.63 and 0.72 to 0.85 and 0.77 for F16
534 and B123, respectively. The classical FAO-dualK_c is based on an estimated SM from a
535 simplified water balance budget (Equation 6), where some water fluxes were neglected in our
536 case (runoff, deep percolation, and capillarity rise…). Where runoff flux takes place above a
537 certain threshold value of soil moisture present in the soil (Manabe, 1969), which can generate
538 some uncertainties. The underestimation of $ET_{c\ act}$ is observed at the beginning of the season,
539 during the germination and emergence stage of growing crops and at the end (senescent stage)
540 of the agricultural season, due to the limitation of the standard FAO-56 model in the estimation
541 of the E_s component where water is lost mainly by E_s.
542 These results are in accordance with several works (Amazirh et al., 2021; Er-Raki et al., 2007;
543 Olivera-Guerra et al., 2018; Rafi et al., 2019). Realistic dynamics of SM allow reflecting
544 correctly the water budget closure to catch the variability of soil E_s. The better results obtained
545 when assimilating SM into FAO-dualK_c confirm this improvement where the integration of SM
546 data allows better control of the model variation, and by assimilation, we tend to adjust soil
547 water content and calibrating FAO-dualK_c model. In the classical FAO, the evaporation
548 coefficient K_e is linked mainly to soil texture based on a standard formulation using SM data
549 (*ad-hoc* relationship with soil texture). This could provide a limitation to some extent in the E_s
550 estimation over bare soil conditions (under/overestimation). By assimilating SM, we tend to
551 correct this issue by adjusting the soil evaporation coefficient, based on a relationship between
552 SM and E_s process taking into account soil types and surface conditions as in Merlin et al.
553 (2018, 2016).
554 Results of the coupled assimilation of SM and LST into FAO-dualK_c for both sites are also
555 given in Table 2. As seen from Table 2, combining LST and SM assimilation schemes provides
556 good results in comparison with standard FAO-dualK_c. The RMSE and the bias are reduced
557 from 0.98 mm/day and -0.47 mm/day to 0.55 mm/day and -0.14 mm/day while R^2 increases

from 0.63 to 0.87 using FAO-dualK_c without assimilation and with assimilation of both SM and LST-proxy conjointly, for F16 site, respectively. These results reveal that the best statistical parameters are provided by jointly assimilating LST_{proxy} and SM data. Looking at the results, for B123 site, it is noticed that the best results are provided when assimilating SM and LST couple with an RMSE of 0.71 mm/day and MBE equal to 0.03 mm/day. While before assimilation, the RMSE and MBE values for the $ET_{c\ act}$ were 1.01 and -0.44 mm/day for the B123 field, respectively. In the case of assimilating SM and LST couple, the effectiveness of the assimilation process is mainly dominated by SM assimilation. Overall, the assimilation approaches provide better results than the standard FAO-56. For F16 sites as an example, the main discrepancies between $ET_{c\ act}$ estimates before and after assimilation can be observed during the development (between December 2015 to January 31, 2016) and late (from 10 May to the end of the season) stages due to great differences in K_e estimates and thus in E_s. Late in the season, a difference is observed between E_s estimates before and after the assimilation procedure. In the standard FAO which is based on daily water balance, the water in the surface evaporable layer is fully depleted means $K_{e,FAO} \sim 0$, and $E_s \approx 0$.. Whereas, when assimilating SM, we tend to update the K_e, and then the evaporation increases to catch better the EC observations. The increase in E_s can be explained by an increase of the sun-exposed soil due to the reduction of vegetation and the capillary rise from the root zone, which can be detected from the SM assimilated into the E_s estimates. Moreover, the underestimation of E_s by FAO-56 could be explained by the definition of the depth of Ze, where a 5 cm SM was used in this study to be consistent with the remote sensing depth. As FAO suggested, Ze should be ranging from 0.10-0.15 cm based on the soil texture and this could affect the final result of E_s estimation as shown previously in Amazirh et al. (2021).

4.3. Assimilating remote sensing data into FAO-dualKc

To evaluate the spatial extensibility of the assimilation scheme, the daily $ET_{c\ act}$ over the selected F16 field during 2015–2016 was simulated at a spatial resolution of 100 m. Only F16 was chosen for the spatial analysis due to the availability of thermal data at high spatio-temporal resolution as Landsat 7 and 8 data as well as SM data derived from SMAP. In this case, SM data was derived from SMAP data product, which were disaggregated to 100 m (Ojha et al., 2019), and LST data were derived from Landsat-7 and Landsat-8 data. As the *in situ* evaluation, two assimilation techniques were tested: SM only and assimilating jointly SM and LST_{proxy} couple into FAO model. Figures 7 and 8 present the scatter and time series plots of the obtained results using the assimilation techniques, respectively.

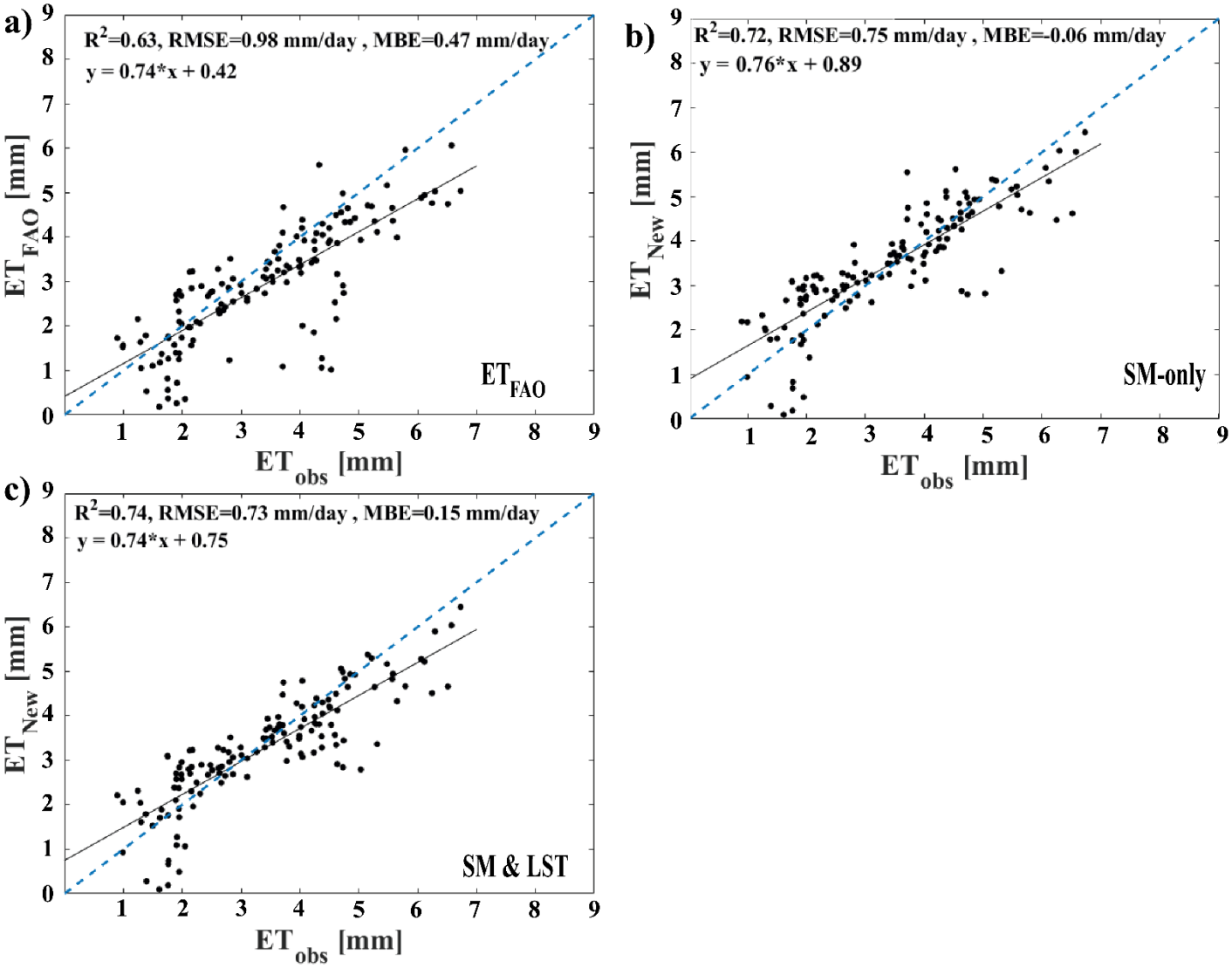

Figure 7: Scatter plot comparison between FAO-dualK_c and observed $ET_{c\ act}$ (ET_{obs}) without assimilation 'ET_{FAO}' (a), when assimilating only soil moisture 'SM-only' (b) and conjointly soil moisture and land surface temperature 'SM and LST' (c).

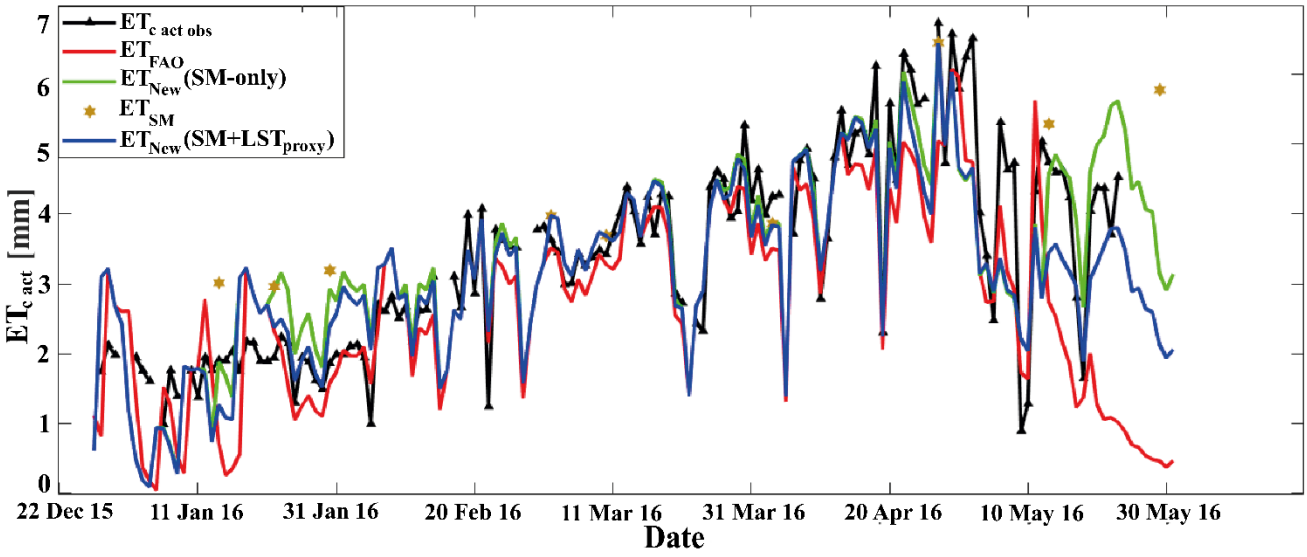

Figure 8: Daily temporal comparison between FAO-dualK_c and observed $ET_{c\ act}$ (ET_{obs}) without assimilation and when assimilating SM-only (SM_{New} (SM-only)) and conjointly SM and LST-proxy (SM_{New} (SM + LST_{proxy})). The ET_{SM} is presented also (yellow hexagram) indicating the assimilation dates.

From the obtained results in Figures 7 and 8, the assimilation approaches tend to improve the $ET_{c\ act}$ estimates either using the proposed assimilation approaches. In the first case, the $SM_{DISPATCH}$ products are only assimilated into FAO-dualK_c. Figures 7 and 8 compare the results of the assimilation procedure with the one from the open-loop ET_{FAO} (no assimilation, Figure 7a and Figure 8 'red line'). When assimilating the SMAP based disaggregated $SM_{DISPATCH}$ (Figure 7b and Figure 8 'green line'), the $ET_{c\ act}$ estimates is improved where the error is reduced compared to ET_{FAO} from 0.98 mm/day to 0.75 mm/day, as well as the bias decreased from -0.47 mm/day to -0.06 mm/day. For the other case, when coupled assimilation of $SM_{DISPATCH}$ and LST through using the normalized LST proxy, the RMSE is equal to 0.73 mm/day with a bias that doesn't exceed 0.15 mm/day. Comparing both assimilation approaches, the lowest RMSE is assessed by assimilating both SM and LST into FAO model (Figure 7c and Figure 8 'blue line'). Without assimilation (ET_{FAO}), FAO-dualK_c severely underestimates $ET_{c\ act}$ during the senescence period (Figure 7a), where both assimilation experiments have slightly similar accuracy in $ET_{c\ act}$ estimates. This is seen especially at the beginning and the end of the wheat growing season (Figure 8), where the SM improves the soil E_s when soil is under bare soil conditions.

We note that the assimilation using *in situ* data provided better and more accurate results than using remote sensing ones. This is due first to the data, where *in situ* data are the truth

observations while the remotely sensed ones are estimated from model (Dispatch for SM) or corrected (MODTRAN for LST) which generate a cumulated error. In this study a proxy of LST was used, therefore the observed error of 2.16 °C when comparing Landsat LST and *in situ* LST may less impact the $ET_{c\ act}$ results since a relative value of LST data (between 0-1) was used. Then the frequency of the *in situ* perturbations (observations) is higher than the remote sensing data (cloud effects and satellite revisit time). This could also impact the results, where the higher assimilation frequency (sequence), the better the $ET_{c\ act}$ estimates are, as found in Er-raki et al., (2008) and Fu et al. (2018). The assimilation of SM allows the updating of the surface depletion (D_e), thus controlling the water budget at the surface then updating the K_e coefficient of evaporation. By integrating the LST information, this allows the updating of the root zone depletion D_r, which controls the temporal course of the root zone water budget, which leads to correcting the K_s values. The idea of assimilating LST into the stress coefficient is to improve the transpiration component. Both sites were well irrigated, and the stress appears just in some periods during the investigated study. The real impact of LST on the water balance at the root zone could be seen clearly in the case of a field that undergoes several stress periods when irrigation is deliberately cut. In this study, just on some dates that the field is undergoing stress period and by assimilating LST into FAO model we succeeded to capture the stress periods. To better observe the difference on the assimilated $K_{e,SM}$ and the surface water balance based $K_{e,FAO}$, Figure 9 illustrates the temporal course comparison between the estimated K_e by FAO-dualK_c model without and with SM assimilation during 2015-2016 growing season for F16 field.

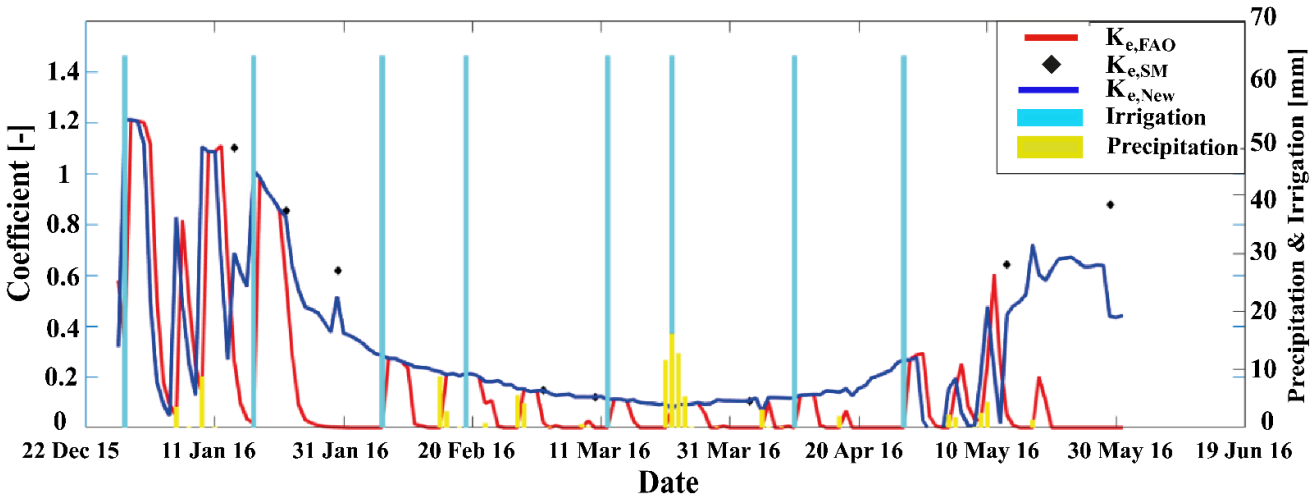

Figure 9: Comparison between the FAO-dualK_c evaporation coefficient $K_{e,FAO}$ before assimilation (red line) and the updated one ($K_{e,New}$) after assimilation (blue line). The $K_{e,SM}$ is

presented also (black rectangles) indicating the assimilation dates. Precipitation and irrigation events are shown as yellow and light blue bars, respectively.

As seen from Figure 9, K_e ranges from 0 to 1.2 for both cases. Nine available dates are used for the SM assimilation when SMAP $SM_{DISPATCH}$ data are available. For dry conditions (absence of irrigation or precipitation, e.g. from the 15th to 31st of January), an increase in the surface depletion leads to a decrease of both K_e and an increase of E_s surface resistance, which induces water stress at the surface. While, after an irrigation or rainfall, soil evaporates at a potential rate when the soil resistance is decreasing, which leads to an increase of K_e. From Figure 9, the daily pattern of $K_{e,FAO}$, and $K_{e,New}$ are similar and responds perfectly to water supply (precipitation or irrigation). Despite that, the assimilated $K_{e,New}$ is more physical which means it increased and decreased progressively, especially during the dryness period. This clearly appears at the 22nd and 11th of January, where the $K_{e,FAO}$ decreased sharply and suddenly than the $K_{e,New}$ that decreased gradually and slowly. It can be concluded that SM assimilation tends to adjust the duration of the dryness phenomena when the water content in the upper soil becomes limiting, taken into account the soil properties as shown in Amazirh et al. (2021). Especially in stage 2 when soil moisture is the limiting factor, the $K_{e,New}$ decreases progressively depending on the soil properties, this because of the response and the soil drying time which is well taken into account in the $K_{e,New}$ approach. For the coupled assimilation, the $K_{e,New}$ was taken to update the E_s component, while the introduction of LST data will update the stress coefficient K_s. Figure 10 shows the time variation comparison between the estimated K_s by FAO-56 model with assimilation ($K_{s,New}$) and without assimilation ($K_{s,FAO}$).

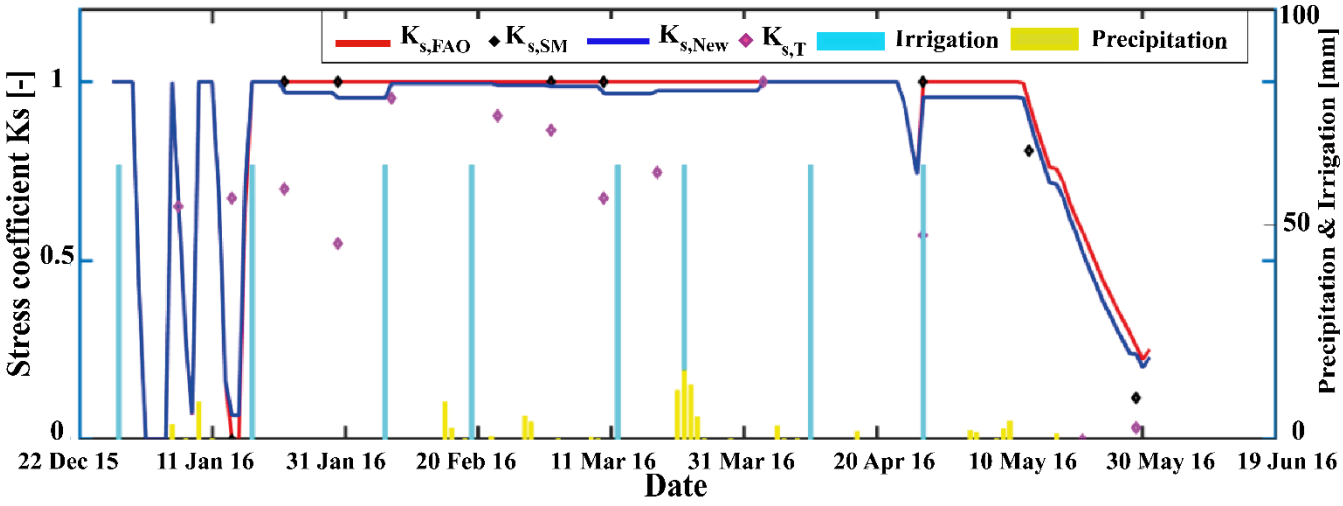

Figure 10: Comparison between the FAO-dualK_c stress coefficient $K_{s,FAO}$ before assimilation (red line) and the updated one ($K_{s,New}$) after assimilating LST_{proxy} and SM couple (blue line).

The $K_{s,SM}$ (black diamonds) and $K_{s,T}$ (pink diamonds) are presented indicating the SM and LST assimilation dates, respectively.

Looking at Figure 10, it can be seen that the $K_{s,FAO}$, and $K_{s,New}$ follow the same variation and in some cases are superposed. K_s reached the value 1 when the D_r is lower than RAW, these cases appeared when the water is supplied by rain or irrigation (Figure 10). When the water supply is insufficient or ET_0 is very high, the root zone depletion increased, and the K_s value dropped below the value 1, which generated wheat stress. The removal of water by $ET_{c\ act}$ leads to activation and an increasing in wheat stomatal resistance as well as an increasing in soil water depletion, and this induced water stress conditions. $K_{s,New}$ simulates stress conditions in a more pronounced way than the classical FAO-dualK_c. Both K_s before and after assimilation responded to water supply and reach the value 1. The main discrepancies between both methods are observed when K_s dropped below 1, where the $K_{s,FAO}$ abruptly decreased while $K_{s,New}$ decreased progressively.

As seen, the flood-irrigated field (F16) was irrigated every 1 to 3 weeks depending on precipitation and a sum of 8 irrigations were observed. Generally, the field was well irrigated and under minimal stress. This makes quantifying the impact of assimilating LST into the FAO-$ET_{c\ act}$ estimation difficult. However, the stress periods were detected when assimilating LST into K_s.

Conclusions

The investigated work deals with improving actual crop evapotranspiration ($ET_{c\ act}$) estimates using data assimilation techniques. The idea was to improve the accuracy of the FAO-dualK_c ET components through assimilating remote sensing data. Surface soil moisture (SM) data is assimilated in order to update soil evaporation and land surface temperature (LST) is assimilated to update the crop wheat transpiration ($T_{c\ act}$). *In situ* SM and LST data are firstly assimilated at the point scale. Then SMAP disaggregated SM and Landsat derived LST was used at field scale. The investigated techniques were tested over two different fields in central Morocco, during the 2002-2003 and 2015-2016 wheat growing seasons, respectively. Our results point out that by assimilating only the SM data, we yield a very satisfying estimation of $ET_{c\ act}$. The modelled $ET_{c\ act}$ tracks successfully the $ET_{c\ act}$ observation. By coupling SM and LST assimilation, the $ET_{c\ act}$ estimates are slightly improved compared to assimilating only SM data. However, some uncertainties were observed, and this could be due to the sensing depth of SM data. The assimilation technique has demonstrated the potential of inferring valuable information from remotely sensed land surface data (SM and LST) for evaluating distributed

water balance models, given that forcing data (including irrigation) are accurately known. The proposed study showed its capability to retrieve $ET_{c\ act}$ at field scale, a spatialization of $ET_{c\ act}$ is needed. This could be done by using LST and SM products at high resolution (Amazirh et al., 2019; Ojha et al., 2019). Recently, Amazirh et al. (2021) proposed a new E_s formulation by including the soil texture information into the reduction coefficient (K_r). The proposed formulation demonstrates its better performance than the classical FAO. Combining the assimilation of SM into E_s formulation developed in Amazirh et al. (2021) could provide more accurate results by improving the E_s component.

Declaration of competing interest

The authors declare that they have no known competing financial interests or personal relationships that could have appeared to influence the work reported in this paper.

Acknowledgements

This study was conducted within the Center of remote sensing applications (https://crsa.um6p.ma/), at the Mohammed VI university-Morocco and funded by OCP (AS No 71). This work was also partly funded by the European Commission Horizon 2020 Programme for Research and Innovation (H2020) in the context of the Marie Sklodowska-Curie Research and Innovation Staff Exchange (RISE) action (REC project, grant agreement no: 645642), followed by ACCWA project, grant agreement no. 823965). The *in situ* data set was provided by the Joint International Laboratory TREMA (http://trema.ucam.ac.ma). PRIMA IDEWA and ALTOS projects are also acknowledged.

References

Abbaszadeh, P., Moradkhani, H., Zhan, X., 2019. Downscaling SMAP Radiometer Soil Moisture Over the CONUS Using an Ensemble Learning Method. Water Resour. Res. 55, 324–344. doi:10.1029/2018WR023354

Abdolghafoorian, A., Farhadi, L., 2020. LIDA: A Land Integrated Data Assimilation Framework for Mapping Land Surface Heat and Evaporative Fluxes by Assimilating Space-Borne Soil Moisture and Land Surface Temperature. Water Resour. Res. 56. doi:10.1029/2020WR027183

Alberto, M.C.R., Quilty, J.R., Buresh, R.J., Wassmann, R., Haidar, S., Correa, T.Q., Sandro, J.M., 2014. Actual evapotranspiration and dual crop coefficients for dry-seeded rice and hybrid maize grown with overhead sprinkler irrigation. Agric. Water Manage. 136, 1–12. doi:10.1016/j.agwat.2014.01.005

Alfieri, J.G., Kustas, W.P., Anderson, M.C., 2018. A Brief Overview of Approaches for Measuring Evapotranspiration, in: Agroclimatology: Linking Agriculture to Climate. pp. 109–127. doi:10.2134/agronmonogr60.2016.0034

Allen, R.G., Pereira, L.S., Howell, T.A., Jensen, M.E., 2011. Evapotranspiration information reporting: I. Factors governing measurement accuracy. Agric. Water Manage. 98, 899–920. doi:10.1016/j.agwat.2010.12.015

Allen, R.G., Pereira, L.S., Raes, D., Smith, M., 1998. Crop evapotranspiration - Guidelines for computing crop water requirements - FAO Irrigation and drainage, Paper No. 56, FAO. Rome, Italy.

Amazirh, A., Er-Raki, S., Chehbouni, A., Rivalland, V., Diarra, A., Khabba, S., Ezzahar, J., Merlin, O., 2017. Modified Penman–Monteith equation for monitoring evapotranspiration of wheat crop: Relationship between the surface resistance and remotely sensed stress index. Biosyst. Eng. 164, 68–84. doi:10.1016/j.biosystemseng.2017.09.015

Amazirh, A., Merlin, O., Er-Raki, S., 2019. Including Sentinel-1 radar data to improve the disaggregation of MODIS land surface temperature data. ISPRS J. Photogramm. Remote Sens. 150, 11–26. doi:10.1016/j.isprsjprs.2019.02.004

Amazirh, A., Merlin, O., Er-Raki, S., Bouras, E., Chehbouni, A., 2021. Implementing a new texture-based soil evaporation reduction coefficient in the FAO dual crop coefficient method. Agric. Water Manage. 250, 106827. doi:10.1016/j.agwat.2021.106827

Amazirh, A., Merlin, O., Er-Raki, S., Gao, Q., Rivalland, V., Malbeteau, Y., Khabba, S., Escorihuela, M.J., 2018. Retrieving surface soil moisture at high spatio-temporal resolution from a synergy between Sentinel-1 radar and Landsat thermal data: A study case over bare soil. Remote Sens. Environ. 211, 321–337. doi:10.1016/j.rse.2018.04.013

ASCE-EWRI, 2004. The ASCE Standardized Reference Evapotranspiration Equation. American Society of Civil Engineers, Reston, VA. doi:10.1061/9780784408056

Baldocchi, D.D., Hicks, B.B., Meyers, T.P., Hincks, B.B., Meyers, T.P., 1988. Measuring biosphere-atmosphere exchanges of biologically related gases with micrometeorological methods. Ecology 69, 1331–1340. doi:10.2307/1941631

Barker, J.B., Heeren, D.M., Neale, C.M.U., Rudnick, D.R., 2018. Evaluation of variable rate irrigation using a remote-sensing-based model. Agric. Water Manage. 203, 63–74. doi:10.1016/j.agwat.2018.02.022

Bateni, S.M., Entekhabi, D., 2012. Surface heat flux estimation with the ensemble Kalman smoother: Joint estimation of state and parameters. Water Resour. Res. 48. doi:10.1029/2011WR011542

Bhattarai, N., Mallick, K., Stuart, J., Vishwakarma, B.D., Niraula, R., Sen, S., Jain, M., 2019. An automated multi-model evapotranspiration mapping framework using remotely sensed and reanalysis data. Remote Sens. Environ. 229, 69–92. doi:10.1016/j.rse.2019.04.026

Bos, M.G., Kseklik, rob A.L., Allen, R.G., Molden, D.J., 2008. Water Requirements for Irrigation and the Environment. doi:10.1007/978-1-4020-8948-0

Boulet, G., Rafi, Z., Le Dantec, V., Mallick, K., Olioso, A., Er-Raki, S., Merlin, O., 2019. Evapotranspiration and Evaporation/Transpiration Retrieval Using Dual-Source Surface Energy Balance Models Integrating VIS/NIR/TIR Data with Satellite Surface Soil Moisture Information. IGARSS 2019 - 2019 IEEE Int. Geosci. Remote Sens. Symp. 6283–6286. doi:10.1109/igarss.2019.8900333

Burba, G., 2013. Eddy Covariance Method-for Scientific, Industrial, Agricultural, and Regulatory Applications, LI-COR Biosciences. doi:10.13140/RG.2.1.4247.8561

Caparrini, F., Castelli, F., Entekhabi, D., 2004. Estimation of surface turbulent fluxes through assimilation of radiometric surface temperature sequences. J. Hydrometeorol. 5, 145–159. doi:10.1175/1525-7541(2004)005<0145:EOSTFT>2.0.CO;2

Chehbouni, A., Escadafal, R., Duchemin, B., Boulet, G., Simonneaux, V., Dedieu, G., Mougenot, B., Khabba, S., Kharrou, H., Maisongrande, P., Merlin, O., Chaponnière, A., Ezzahar, J., Er-Raki, S., Hoedjes, J., Hadria, R., Abourida, A., Cheggour, A., Raibi, F., Boudhar, A., Benhadj, I., Hanich, L., Benkaddour, A., Guemouria, N., Chehbouni, A.H.,

Lahrouni, A., Olioso, A., Jacob, F., Williams, D.G., Sobrino, J. a, 2008. An integrated modelling and remote sensing approach for hydrological study in arid and semi-arid regions: the SUDMED Programme. Int. J. Remote Sens. 29, 5161–5181. doi:10.1080/01431160802036417

Chen, S., Qi, J., Sun, X., Deng, X., Tian, J., 2013. An evapotranspiration assimilation method based on ensemble kalman filter and À trous wavelet. Adv. Meteorol. 2013. doi:10.1155/2013/531810

Courtier, P., Derber, J., Errico, R., Louis, J., Vukicevic, T., 1993. Important literature on the use of adjoint, variational methods and the Kalman filter in meteorology. Tellus A 45, 342–357. doi:10.1034/j.1600-0870.1993.t01-4-00002.x

Dee, D., Uppala, S., Simmons, A., Berrisford, P., Poli, P., Kobayashi, S., Andrae, U., Balmaseda, M., Balsamo, G., Bauer, P., 2011. The ERA - Interim reanalysis: Configuration and performance of the data assimilation system. Quaterly J. R. Meteorol. Soc. 137, 553–597. doi:10.1002/qj.828

DeJonge, K.C., Taghvaeian, S., Trout, T.J., Comas, L.H., 2015. Comparison of canopy temperature-based water stress indices for maize. Agric. Water Manage. 156, 51–62. doi:10.1016/j.agwat.2015.03.023

Drerup, P., Brueck, H., Scherer, H.W., 2017. Evapotranspiration of winter wheat estimated with the FAO 56 approach and NDVI measurements in a temperate humid climate of NW Europe. Agric. Water Manage. 192, 180–188. doi:10.1016/j.agwat.2017.07.010

Elfarkh, J., Er-Raki, S., Ezzahar, J., Chehbouni, A., Aithssaine, B., Amazirh, A., Khabba, S., Jarlan, L., 2021. Integrating thermal stress indexes within Shuttleworth–Wallace model for evapotranspiration mapping over a complex surface. Irrig. Sci. 39, 45–61. doi:10.1007/s00271-020-00701-3

Entekhabi, D., Yueh, Si., O'Neil, P.E., Kellogg, K.H., Allen, A., Bindlish, R., Administration, N.A. and S., 2014. SMAP Handbook–Soil Moisture Active Passive: Mapping Soil Moisture and Freezs/Thaw from Space. Jet Propulsion Laboratory, Pasadena, CA, USA.

Er-Raki, S., Chehbouni, A., Ezzahar, J., Khabba, S., Lakhal, E.K., Duchemin, B., 2011. Derived crop coefficients for winter wheat using different reference evapotranspiration estimates methods. J. Agric. Sci. Technol. 13, 209–221.

Er-Raki, S., Chehbouni, A., Guemouria, N., Duchemin, B., Ezzahar, J., Hadria, R., 2007. Combining FAO-56 model and ground-based remote sensing to estimate water consumptions of wheat crops in a semi-arid region. Agric. Water Manage. 87, 41–54. doi:10.1016/j.agwat.2006.02.004

Er-Raki, S., Chehbouni, A., Hoedjes, J., Ezzahar, J., Duchemin, B., Jacob, F., 2008. Improvement of FAO-56 method for olive orchards through sequential assimilation of thermal infrared-based estimates of ET. Agric. Water Manag. 95, 309–321. doi:10.1016/j.agwat.2007.10.013

Er-Raki, S., Ezzahar, J., Khabba, S., Jarlan, L., Kharrou, M.H., Chehbouni, G., 2013. Micrometeorology tools for measuring evapotranspiration from the leaf to the region, in: Evapotranspiration: Processes, Sources and Environmental Implications. New York : Nova Science, (Environmental Science, Engineering and Technology), pp. 1–22.

Ezzahar, J., Chehbouni, A., 2009. The use of scintillometry for validating aggregation schemes over heterogeneous grids. Agric. For. Meteorol. 149, 2098–2109. doi:10.1016/J.AGRFORMET.2009.09.004

French, A.N., Hunsaker, D.J., Sanchez, C.A., Saber, M., Gonzalez, J.R., Anderson, R., 2020. Satellite-based NDVI crop coefficients and evapotranspiration with eddy covariance validation for multiple durum wheat fields in the US Southwest. Agric. Water Manage. 239. doi:10.1016/j.agwat.2020.106266

French, A.N., Hunsaker, D.J., Thorp, K.R., 2015. Remote sensing of evapotranspiration over

836 cotton using the TSEB and METRIC energy balance models. Remote Sens. Environ. 158,
837 281–294. doi:10.1016/j.rse.2014.11.003
838 Fu, X., Yu, Z., Ding, Y., Tang, Y., Lu, H., 2018. Analysis of influence of observation operator
839 on sequential data assimilation through soil temperature simulation with common land
840 model. Water Sci. Eng. 11, 196–204. doi:10.1016/j.wse.2018.09.003
841 Gerhards, M., Schlerf, M., Mallick, K., Udelhoven, T., 2019. Challenges and future
842 perspectives of multi-/Hyperspectral thermal infrared remote sensing for crop water-stress
843 detection: A review. Remote Sens. 11. doi:10.3390/rs11101240
844 Gokmen, M., Vekerdy, Z., Verhoef, A., Verhoef, W., Batelaan, O., van der Tol, C., 2012.
845 Integration of soil moisture in SEBS for improving evapotranspiration estimation under
846 water stress conditions. Remote Sens. Environ. 121, 261–274.
847 doi:10.1016/j.rse.2012.02.003
848 Granger, R.., 2000. Satellite-derived estimates of evapotranspiration in the Gediz basin. J.
849 Hydrol. 229, 70–76. doi:10.1016/S0022-1694(99)00200-0
850 He, X., Xu, T., Bateni, S.M., Neale, C.M.U., Liu, S., Auligne, T., Wang, K., Zhu, S., 2019.
851 Mapping Regional Turbulent Heat Fluxes via Assimilation of MODIS Land Surface
852 Temperature Data into an Ensemble Kalman Smoother Framework. Earth Sp. Sci. 6.
853 doi:10.1029/2019EA000705
854 Idso, S.B., Jackson, R.D., Pinter, P.J., Reginato, R.J., Hatfield, J.L., 1981. Normalizing the
855 stress-degree-day parameter for environmental variability. Agric. Meteorol.
856 doi:10.1016/0002-1571(81)90032-7
857 Ihuoma, S.O., Madramootoo, C.A., 2017. Recent advances in crop water stress detection.
858 Comput. Electron. Agric. 141, 267–275. doi:10.1016/j.compag.2017.07.026
859 Kalma, J.D., McVicar, T.R., McCabe, M.F., 2008. Estimating land surface evaporation: A
860 review of methods using remotely sensed surface temperature data. Surv. Geophys. 29,
861 421–469. doi:10.1007/s10712-008-9037-z
862 Kharrou, M.H., Le Page, M., Chehbouni, A., Simonneaux, V., Er-Raki, S., Jarlan, L., Ouzine,
863 L., Khabba, S., Chehbouni, G., 2013. Assessment of Equity and Adequacy of Water
864 Delivery in Irrigation Systems Using Remote Sensing-Based Indicators in Semi-Arid
865 Region, Morocco. Water Resour. Manage. 27, 4697–4714. doi:10.1007/s11269-013-0438-
866 5
867 Ko, J., Piccinni, G., Marek, T., Howell, T., 2009. Determination of growth-stage-specific crop
868 coefficients (Kc) of cotton and wheat. Agric. Water Manage. 96, 1691–1697.
869 doi:10.1016/j.agwat.2009.06.023
870 Kohsiek, W., Meijninger, W.M.L., Moene, A.F., Heusinkveld, B.G., Hartogensis, O.K., Hillen,
871 W.C.A.M., De Bruin, H.A.R., 2002. An Extra Large Aperture Scintillometer For Long
872 Range Applications. Boundary-Layer Meteorol. 105, 119–127.
873 doi:10.1023/A:1019600908144
874 Kullberg, E.G., DeJonge, K.C., Chávez, J.L., 2017. Evaluation of thermal remote sensing
875 indices to estimate crop evapotranspiration coefficients. Agric. Water Manage. 179, 64–
876 73. doi:10.1016/j.agwat.2016.07.007
877 Kumar, S. V., Reichle, R.H., Peters-Lidard, C.D., Koster, R.D., Zhan, X., Crow, W.T.,
878 Eylander, J.B., Houser, P.R., 2008. A land surface data assimilation framework using the
879 land information system: Description and applications. Adv. Water Resour. 31, 1419–
880 1432. doi:10.1016/j.advwatres.2008.01.013
881 Kustas, W.P., Norman, J.M., 1996. Use of remote sensing for evapotranspiration monitoring
882 over land surfaces. Hydrol. Sci. J. 41, 495–516. doi:10.1080/02626669609491522
883 Li, Z.-L.L., Tang, R., Wan, Z., Bi, Y., Zhou, C., Tang, B., Yan, G., Zhang, X., Li, Z.-L.L.,
884 Tang, R., Wan, Z., Bi, Y., Zhou, C., Tang, B., Yan, G., Zhang, X., 2009. A review of
885 current methodologies for regional Evapotranspiration estimation from remotely sensed

886 data. Sensors 9, 3801–3853. doi:10.3390/s90503801
887 Littell, J.S., Peterson, D.L., Riley, K.L., Liu, Y., Luce, C.H., 2016. A review of the relationships
888 between drought and forest fire in the United States. Glob. Chang. Biol. 22, 2353–2369.
889 doi:10.1111/gcb.13275
890 Liu, Y., Luo, Y., 2010. A consolidated evaluation of the FAO-56 dual crop coefficient approach
891 using the lysimeter data in the North China Plain. Agric. Water Manage. 97, 31–40.
892 doi:10.1016/j.agwat.2009.07.003
893 Madugundu, R., Al-Gaadi, K.A., Tola, E.K., Hassaballa, A.A., Patil, V.C., 2017. Performance
894 of the METRIC model in estimating evapotranspiration fluxes over an irrigated field in
895 Saudi Arabia using Landsat-8 images. Hydrol. Earth Syst. Sci. 21, 6135–6151.
896 doi:10.5194/hess-21-6135-2017
897 McLaughlin, D., Zhou, Y., Entekhabi, D., Chatdarong, V., 2006. Computational issues for
898 large-scale land surface data assimilation problems. J. Hydrometeorol. 7, 494–510.
899 doi:10.1175/JHM493.1
900 Merlin, O., Chehbouni, A., Boulet, G., Kerr, Y., 2006. Assimilation of Disaggregated
901 Microwave Soil Moisture into a Hydrologic Model Using Coarse-Scale Meteorological
902 Data. J. Hydrometeorol. 7, 1308–1322. doi:10.1175/JHM552.1
903 Merlin, O., Olivera-guerra, L., Aït Hssaine, B., Amazirh, A., Ra, Z., Ezzahar, J., Gentine, P.,
904 Khabba, S., Gascoin, S., Er-raki, S., 2018. A phenomenological model of soil evaporative
905 e ffi ciency using surface soil moisture and temperature data. Agric. For. Meteorol. 257,
906 501–515. doi:10.1016/j.agrformet.2018.04.010
907 Merlin, O., Stefan, V.G.V.G.G., Amazirh, A., Chanzy, A., Ceschia, E., Er-Raki, S., Gentine,
908 P., Tallec, T., Ezzahar, J., Bircher, S., Beringer, J., Khabba, S., Gentine, P., Er-Raki, S.,
909 Bircher, S., Khabba, S., 2016. Modeling soil evaporation efficiency in a range of soil and
910 atmospheric conditions using ameta-analysis approach. Water Resour. Res. 52, 3663–
911 3684. doi:10.1002/2015WR018233.Received
912 Molden, D., Oweis, T., Steduto, P., Bindraban, P., Hanjra, M.A., Kijne, J., 2010. Improving
913 agricultural water productivity: Between optimism and caution. Agric. Water Manage. 97,
914 528–535. doi:10.1016/j.agwat.2009.03.023
915 Moradkhani, H., Hsu, K.L., Gupta, H., Sorooshian, S., 2005. Uncertainty assessment of
916 hydrologic model states and parameters: Sequential data assimilation using the particle
917 filter. Water Resour. Res. 41, 1–17. doi:10.1029/2004WR003604
918 Neale, C.M.U., Geli, H.M.E., Kustas, W.P., Alfieri, J.G., Gowda, P.H., Evett, S.R., Prueger,
919 J.H., Hipps, L.E., Dulaney, W.P., Chávez, J.L., French, A.N., Howell, T.A., 2012. Soil
920 water content estimation using a remote sensing based hybrid evapotranspiration modeling
921 approach. Adv. Water Resour. 50, 152–161. doi:10.1016/j.advwatres.2012.10.008
922 Ojha, N., Merlin, O., Molero, B., Suere, C., Olivera-Guerra, L., Ait Hssaine, B., Amazirh, A.,
923 Al Bitar, A., Escorihuela, M., Er-Raki, S., 2019. Stepwise Disaggregation of SMAP Soil
924 Moisture at 100 m Resolution Using Landsat-7/8 Data and a Varying Intermediate
925 Resolution. Remote Sens. 11, 1863. doi:10.3390/rs11161863
926 Olioso, A., 1995. Estimating the difference between brightness and surface temperatures for a
927 vegetal canopy. Agric. For. Meteorol. 72, 237–242. doi:10.1016/0168-1923(94)02163-E
928 Olivera-Guerra, L., Merlin, O., Er-Raki, S., Khabba, S., Escorihuela, M.J., 2018. Estimating
929 the water budget components of irrigated crops: Combining the FAO-56 dual crop
930 coefficient with surface temperature and vegetation index data. Agric. Water Manage. 208,
931 120–131. doi:10.1016/j.agwat.2018.06.014
932 Paço, T.A., Pôças, I., Cunha, M., Silvestre, J.C., Santos, F.L., Paredes, P., Pereira, L.S., 2014.
933 Evapotranspiration and crop coefficients for a super intensive olive orchard. An
934 application of SIMDualKc and METRIC models using ground and satellite observations.
935 J. Hydrol. 519. doi:10.1016/j.jhydrol.2014.09.075

936 Paredes, P., Rodrigues, G.C., Alves, I., Pereira, L.S., 2014. Partitioning evapotranspiration,
937 yield prediction and economic returns of maize under various irrigation management
938 strategies. Agric. Water Manage. 135. doi:10.1016/j.agwat.2013.12.010
939 Peng, J., Loew, A., Merlin, O., Verhoest, N.E.C., 2017. A review of spatial downscaling of
940 satellite remotely sensed soil moisture. Rev. Geophys. 55, 341–366.
941 doi:10.1002/2016RG000543
942 Pereira, L.S., Paredes, P., Hunsaker, D.J., López-Urrea, R., Mohammadi Shad, Z., 2021.
943 Standard single and basal crop coefficients for field crops. Updates and advances to the
944 FAO56 crop water requirements method. Agric. Water Manage.
945 doi:10.1016/j.agwat.2020.106466
946 Pereira, L.S., Paredes, P., Jovanovic, N., 2020. Soil water balance models for determining crop
947 water and irrigation requirements and irrigation scheduling focusing on the FAO56
948 method and the dual Kc approach. Agric. Water Manage.
949 doi:10.1016/j.agwat.2020.106357
950 Pipunic, R.C., Walker, J.P., Western, A., 2008. Assimilation of remotely sensed data for
951 improved latent and sensible heat flux prediction: A comparative synthetic study. Remote
952 Sens. Environ. 112, 1295–1305. doi:10.1016/j.rse.2007.02.038
953 Rafi, Z., Merlin, O., Le Dantec, V., Khabba, S., Mordelet, P., Er-Raki, S., Amazirh, A., Olivera-
954 Guerra, L., Ait Hssaine, B., Simonneaux, V., Ezzahar, J., Ferrer, F., 2019. Partitioning
955 evapotranspiration of a drip-irrigated wheat crop: Inter-comparing eddy covariance-, sap
956 flow-, lysimeter- and FAO-based methods. Agric. For. Meteorol. 265, 310–326.
957 doi:10.1016/j.agrformet.2018.11.031
958 Rosa, R.D., Paredes, P., Rodrigues, G.C., Alves, I., Fernando, R.M., Pereira, L.S., Allen, R.G.,
959 2012a. Implementing the dual crop coefficient approach in interactive software. 1.
960 Background and computational strategy. Agric. Water Manage. 103.
961 doi:10.1016/j.agwat.2011.10.013
962 Rosa, R.D., Paredes, P., Rodrigues, G.C., Fernando, R.M., Alves, I., Pereira, L.S., Allen, R.G.,
963 2012b. Implementing the dual crop coefficient approach in interactive software: 2. Model
964 testing. Agric. Water Manage. 103. doi:10.1016/j.agwat.2011.10.018
965 Rosenberg, N.J., Blad, B.L., Verma, S.B., 1983. Microclimate. The Biological Environment (2
966 nd edition), Wiley–Blac. ed.
967 Schuurmans, J.M., Troch, P.A., Veldhuizen, A.A., Bastiaanssen, W.G.M., Bierkens, M.F.P.,
968 2003. Assimilation of remotely sensed latent heat flux in a distributed hydrological model.
969 Adv. Water Resour. 26, 151–159. doi:10.1016/S0309-1708(02)00089-1
970 Seguin, B., Itier, B., 1983. Using midday surface temperature to estimate daily evaporation
971 from satellite thermal IR data. Int. J. Remote Sens. 4, 371–383.
972 doi:10.1080/01431168308948554
973 Stanev, E., Schulz-Stellenfleth, J., 2014. Methods of data assimilation. Kuste 133–151.
974 Tajfar, E., Bateni, S.M., Lakshmi, V., Ek, M., 2020. Estimation of surface heat fluxes via
975 variational assimilation of land surface temperature, air temperature and specific humidity
976 into a coupled land surface-atmospheric boundary layer model. J. Hydrol. 583.
977 doi:10.1016/j.jhydrol.2020.124577
978 Tardy, B., Rivalland, V., Huc, M., Hagolle, O., Marcq, S., Boulet, G., 2016. A Software Tool
979 for Atmospheric Correction and Surface Temperature Estimation of Landsat Infrared
980 Thermal Data. Remote Sens. 8, 696. doi:10.3390/rs8090696
981 Tasumi, M., 2019. Estimating evapotranspiration using METRIC model and Landsat data for
982 better understandings of regional hydrology in the western Urmia Lake Basin. Agric.
983 Water Manage. 226, 105805. doi:10.1016/j.agwat.2019.105805
984 Testi, L., Villalobos, F.., Orgaz, F., 2004. Evapotranspiration of a young irrigated olive orchard
985 in southern Spain. Agric.For.Meteorol 121, 1–18.

doi:10.1016/J.AGRFORMET.2003.08.005
Tian, X., Xie, Z., Dai, A., 2008. An ensemble-based explicit four-dimensional variational assimilation method. J. Geophys. Res. Atmos. 113. doi:10.1029/2008JD010358
Twine, T.E., Kustas, W.P., Norman, J.M., Cook, D.R., Houser, P.R., Meyers, T.P., Prueger, J.H., Starks, P.J., Wesely, M.L., 2000. Correcting eddy-covariance flux underestimates over a grassland. Agric. For. Meteorol. 103, 279–300. doi:10.1016/S0168-1923(00)00123-4
Walker, E., García, G.A., Venturini, V., Carrasco, A., 2019. Regional evapotranspiration estimates using the relative soil moisture ratio derived from SMAP products. Agric. Water Manage. 216, 254–263. doi:10.1016/j.agwat.2019.02.009
Wang, X., Ma, M., Han, X., Song, Y., 2009. Assimilation of soil moisture in LPJ-DGVM. Remote Sens. Agric. Ecosyst. Hydrol. XI 7472, 747220. doi:10.1117/12.830312
Xie, X., Zhang, D., 2010. Data assimilation for distributed hydrological catchment modeling via ensemble Kalman filter. Adv. Water Resour. 33, 678–690. doi:10.1016/j.advwatres.2010.03.012
Xu, T., Bateni, S.M., Margulis, S.A., Song, L., Liu, S., Xu, Z., 2016. Partitioning evapotranspiration into soil evaporation and canopy transpiration via a two-source variational data assimilation system. J. Hydrometeorol. 17, 2353–2370. doi:10.1175/JHM-D-15-0178.1
Xu, T., He, X., Bateni, S.M., Auligne, T., Liu, S., Xu, Z., Zhou, J., Mao, K., 2019. Mapping regional turbulent heat fluxes via variational assimilation of land surface temperature data from polar orbiting satellites. Remote Sens. Environ. 221. doi:10.1016/j.rse.2018.11.023
Xu, T., Liang, S., Liu, S., 2011. Estimating turbulent fluxes through assimilation of geostationary operational environmental satellites data using ensemble Kalman filter. J. Geophys. Res. Atmos. 116. doi:10.1029/2010JD015150
Zribi, M., Chahbi, A., Shabou, M., Lili-Chabaane, Z., Duchemin, B., Baghdadi, N., Amri, R., Chehbouni, A., 2011. Soil surface moisture estimation over a semi-arid region using ENVISAT ASAR radar data for soil evaporation evaluation. Hydrol. Earth Syst. Sci. 15, 345–358. doi:10.5194/hess-15-345-2011